

Article

Lagoonal Microfacies, Lithostratigraphy, Correlation and Shale Migration of the Basal Middle Eocene Seeb Formation (Rusayl Embayment, Sultanate of Oman)

Frank Mattern ^{1,*}, Andreas Scharf ¹ , Abdul Razak Al-Sayigh ¹, Nada Al-Wahaibi ¹, Laura Galluccio ², Gianluca Frijia ³ and Mazin Al-Salmani ¹

¹ Department of Earth Sciences, Sultan Qaboos University, P.O. Box 36, Al-Khod, Muscat 123, Oman; scharfa@zedat.fu-berlin.de (A.S.); alsayigh@squ.edu.om (A.R.A.-S.); nada.wahaibi@gmail.com (N.A.-W.); s100546@student.squ.edu.om (M.A.-S.)

² Badley-Ashton, Winceby House, Winceby, Horncastle, Lincolnshire GB LN9 6PB, UK; lgalluccio@badley-ashton.com

³ Department of Physics and Earth Sciences, University of Ferrara, Via Saragat 1, 44121 Ferrara, Italy; gianluca.frijia@unife.it

* Correspondence: frank@squ.edu.om or fmattern@zedat.fu-berlin.de

Abstract: The study improves the understanding of the basal part of the Eocene Seeb Formation of Oman, informally known as “Unit 1”, in terms of microfacies, lithostratigraphy and shale migration within the context of regional tectonics. We logged four sections bed-by-bed over a distance of 8.3 km, collected samples and analyzed thin-sections as well as XRD samples. For the first time, the microfacies and stratigraphic correlation of the lowermost part of the limestone-dominated Seeb Formation were studied in detail. In the analyzed area, Unit 1 is ~20 to 40 m thick, with the thickness increasing to the SE. In the upper part of Unit 1 is a laterally continuous shale horizon. The limestones of Unit 1 contain mostly packstones and grainstones. The dominant standard microfacies types are SMF 18-FOR and SMF 16. The former is dominated by benthic foraminifera, and the latter by peloids. Both SMFs indicate restricted lagoonal conditions. Foraminifera are common in Unit 1 and indicate a middle Eocene age. Considering the abundance of encountered foraminiferal bioclasts, it appears probable that the lagoon barrier was mainly composed of foraminiferal tests. Gutter casts, slumps and debrites indicate an active, partly unstable syndepositional slope, which was likely initially created by uplift of the Saih Hatat Dome and Jabal Nakhl Subdome. Differential regional uplift due to a more pronounced overall doming in the NW (Jabal Nakhl Subdome) than in the SE (Saih Hatat Dome) explains more accommodation space and greater thickness towards the SE. For the first time, we report visco-plastic shale migration/intrusion within the Seeb Formation, related to a shale horizon of Unit 1. This shale locally migrated as indicated by (1) local thickness variations, (2) detached limestone boulders floating in the shale, (3) limestone beds that have been cut-off by the shale and (4) dragged by the shale (5) an upward shale intrusion/injection which then spread parallelly to bedding similar to a salt tongue and (6) tilting overlying limestones. We suggest that shale migration is related to post-“mid”-Eocene E-W convergence between Arabia and India and to faulting or to the second, late Paleogene/early Neogene, faulting interval of the Frontal Range Fault. The shale horizon in the upper part of Unit 1 is a marker bed, which can be correlated across the study area.

Keywords: Unit 1; gutter cast; debrite; shale intrusion; Jabal Akhdar doming; Saih Hatat doming; rimmed shelf



Citation: Mattern, F.; Scharf, A.; Al-Sayigh, A.R.; Al-Wahaibi, N.; Galluccio, L.; Frijia, G.; Al-Salmani, M. Lagoonal Microfacies, Lithostratigraphy, Correlation and Shale Migration of the Basal Middle Eocene Seeb Formation (Rusayl Embayment, Sultanate of Oman). *Geosciences* **2023**, *13*, 254. <https://doi.org/10.3390/geosciences13090254>

Academic Editors: Olivier Lacombe and Jesus Martinez-Frias

Received: 17 May 2023

Revised: 17 August 2023

Accepted: 18 August 2023

Published: 22 August 2023



Copyright: © 2023 by the authors. Licensee MDPI, Basel, Switzerland. This article is an open access article distributed under the terms and conditions of the Creative Commons Attribution (CC BY) license (<https://creativecommons.org/licenses/by/4.0/>).

1. Introduction

The Seeb Formation is the thickest (600 m) Cenozoic formation of Oman (Figure 1) displaying a wide regional distribution [1], which indicates the importance of this limestone formation. The name “Seeb Formation” (Figure 1) was introduced by Nolan et al. [1]. Based

on unpublished data of R. Crawford (1982, no further bibliographic details mentioned), these authors described the formation from the type section along the Nizwa Highway (also known as the “Nizwa Express Road”; for location, see Figures 2 and 3), where they recorded a basal succession of 30 m thickness made of beige, moderately to thickly bedded, well-bedded calcarenite and cross-bedded limestones, occasionally with milky, white quartz vein pebbles and common miliolids. The basal 6 m of the calcarenite contains abundant echinoids [1]. For the basal part of the formation, Nolan et al. [1] suggested the presence of high-energy shoals. The overlying 51 m (above the calcarenite) is characterized by medium-bedded, bioturbated, nodular packstones with orbitoids, alveolinids, miliolids and occasional *Nummulites* and rhodolithic algae [1]. Nolan et al. [1] interpreted the depositional environment of the Seeb Formation as a shallow, open, carbonate shelf setting with a wide variety of local facies.

The Seeb Formation was assigned to a “mid”-Eocene age based on the analysis of benthic foraminifera and echinoids [review in 1] or of foraminifera only [2,3]. According to Jones and Racey [2], the Seeb Formation of the eastern Oman Mountains contains the corresponding index species *Nummulites obesus* and *Assilina spira abradi* zones of Schaub [4] (Lutetian Inferieur = NP15) and in the Al-Khod area (area around Al-Khod Village), the index species of the late Eocene *N. perforates* Zone (Biarritzian = NP18). The base of the Seeb Formation in the study area dates as “basal Lutetian” as suggested by benthic foraminifera [3]. Thus, the onset of deposition of the Seeb Formation coincides with or somewhat postdates the base of the Lutetian (47.8 Ma, [5]).

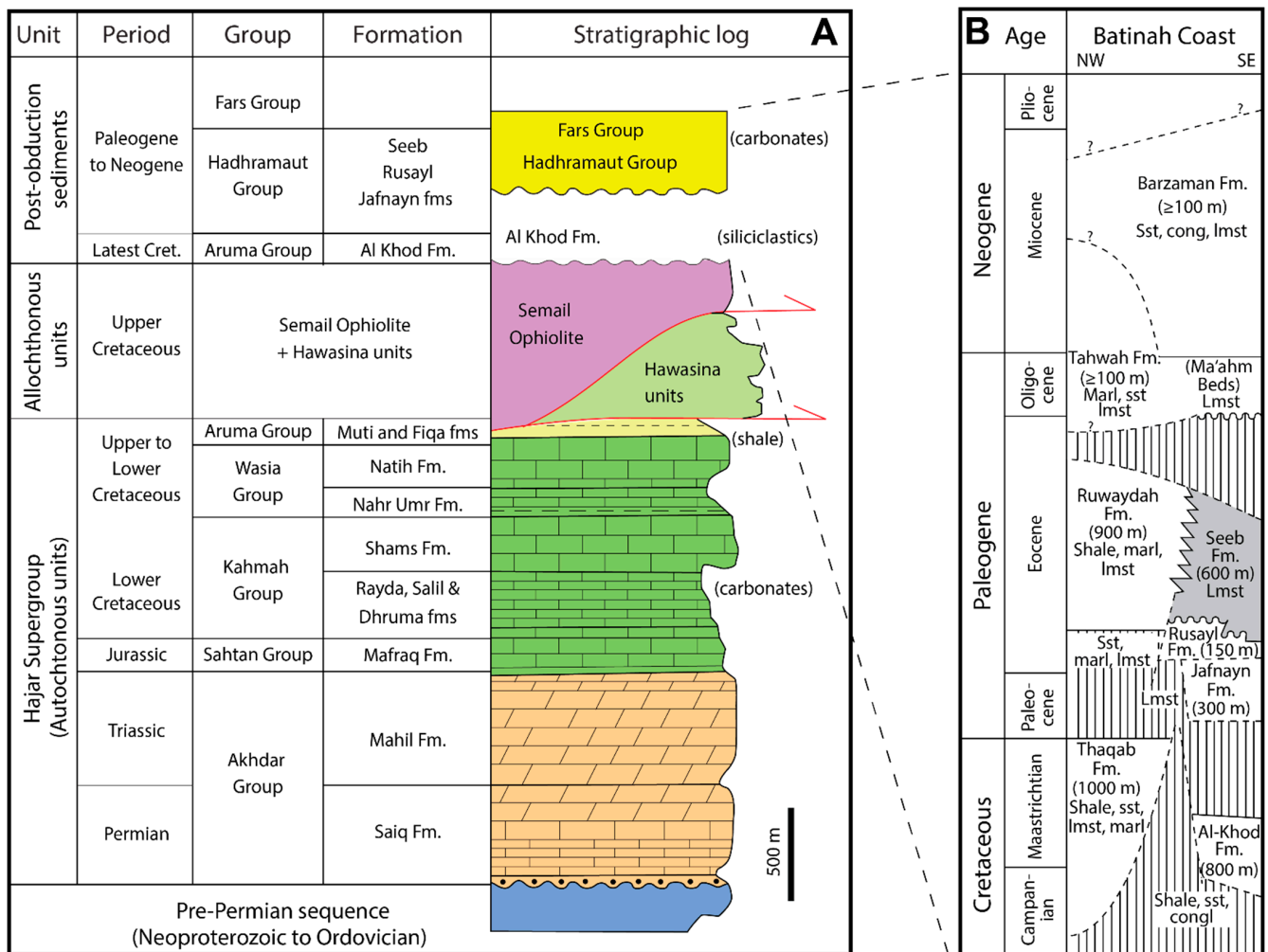


Figure 1. Stratigraphic overview of the study area, emphasizing the post-obductional stratigraphy. (A) Pre-obductional formations (Saiq to Natih formations) and syn-obductional Aruma Group of the

study area, drawn after Béchenec et al. [6]. The Hawasina rocks are deep-sea deposits of Permian to Cretaceous age. The Cretaceous Semail Ophiolite consists mostly of igneous rocks. (B) Post-obductional formations, inspired by various sources [1,3,7–10].

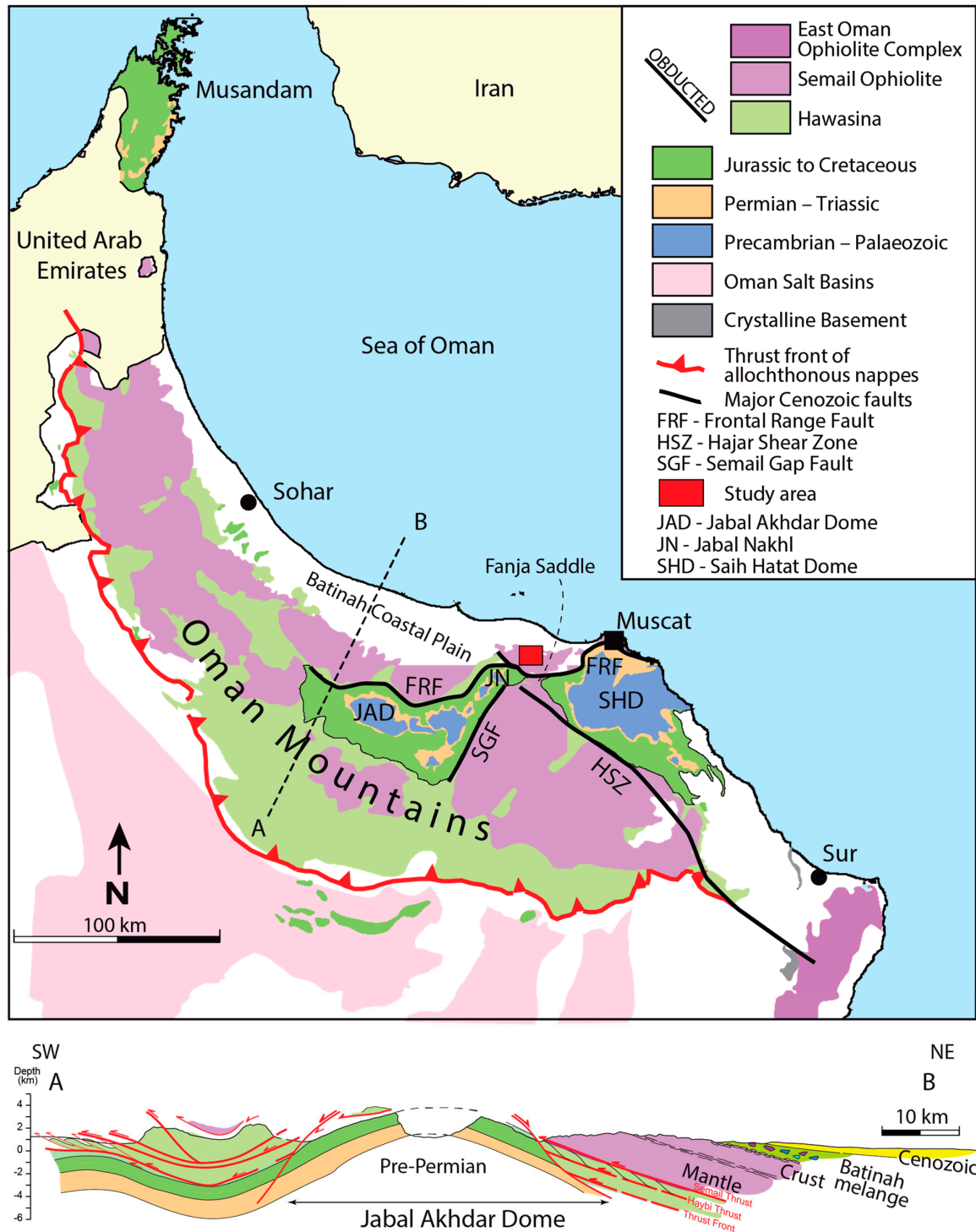


Figure 2. Geological overview map of the Oman Mountains and position of the study area (drawn mainly after Callegari et al. [11]; FRF after Mattern and Scharf, [12]; HSZ after Scharf et al. [13,14]; SGF after Scharf et al. [13]). The two domes are tectonic windows depicting the autochthonous sequence below the allochthonous rocks of the obducted ophiolite and Hawasina rocks. Cross-section simplified after Searle [15].

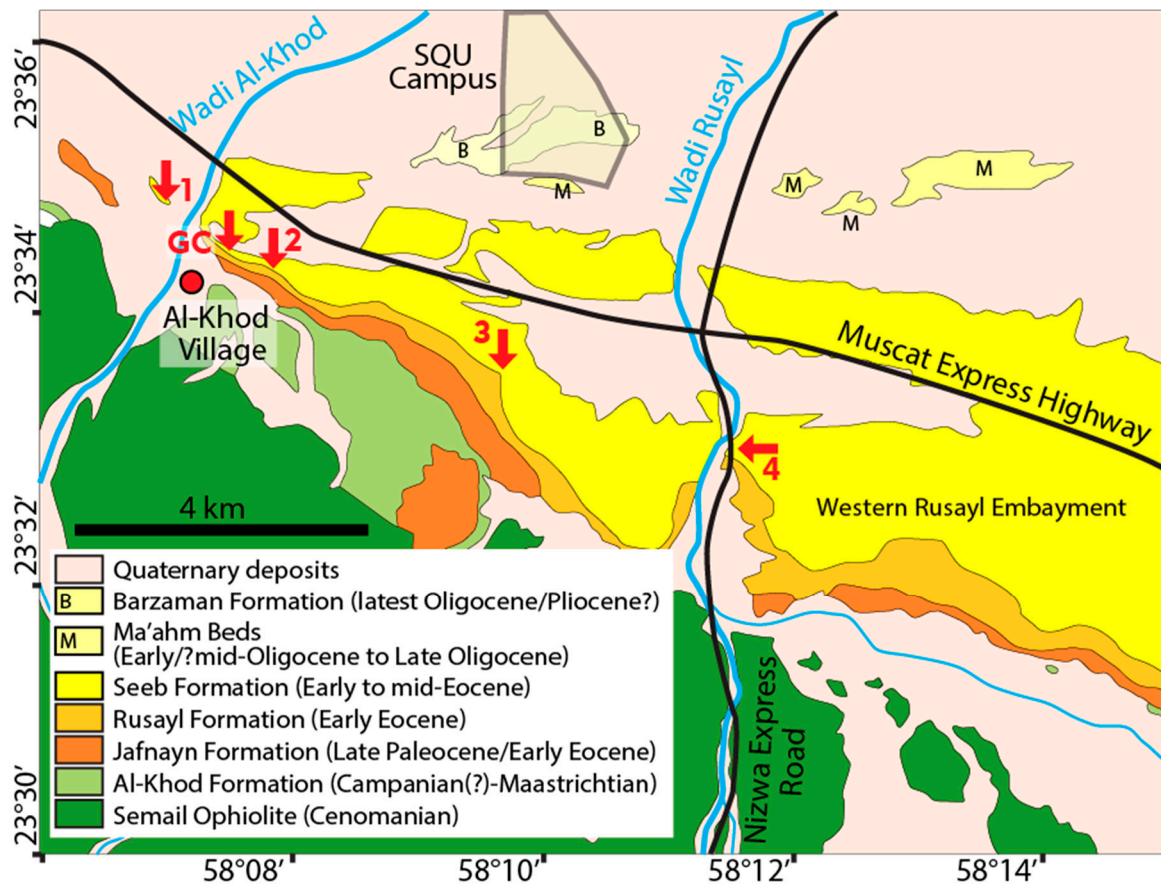


Figure 3. Geological map of the study area known as the “Tertiary Ridge”, represented by the Jafnayn, Rusayl and Seeb formations and positions of the four measured sections (arrows “1” to “4”) and location of the basal gutter cast outcrop (arrow “GC”) in the western part of the Rusayl Embayment. Drawn after Béchenneq et al. [6].

The disconformity between the older Rusayl Formation and the Seeb Formation (Figure 1) was stressed by Béchenneq et al. [6]. They summarized that the basal 50 m of the Seeb Formation comprises nodular, bioclastic limestone containing quartz pebbles and displaying cross-bedding. They also mentioned a microflora of dasycladacean and corallinean algae (*Distychoplax biserialis*) and a microfauna of benthic foraminifera such as *Somalina stephanii*, *Alveolina* sp., *Lockhartia* cf. *hunti*, *Dictyoconus* sp., *Nummulites discorbinus minor*, *Orebitolites* sp. and miliolids, indicating an early Lutetian age. Moreover, they mentioned the presence of syndepositional faults in the basal part of the Seeb Formation.

In the Rusayl Embayment (Figure 3), the basal limestones of the Seeb Formation are well-bedded, graded and low-angle cross-bedded calcarenites, often showing indistinct hummocky cross-stratification [3]. The base of these beds usually contains well-rounded white hydrothermal quartz vein pebbles associated with abundant shallow marine bioclasts such as miliolids and textulariids as well as calcareous green algae, including dasycladaceans and codiaceans [3]. The depositional setting of the Seeb Formation was suggested to be a carbonate ramp, influenced by storm events and wind-wave activity, creating beach barrier complexes through shoreward movement of sand in the lower part of the Seeb Formation [3]. Later work by this author focused on the nummulite accumulations (banks) of the Seeb Formation without being specific with regard to the formation’s basal segment [16], but he mentioned the presence of green algae in the lower part of the formation [16].

Beavington-Penney et al. [7] worked on the lower part of the Seeb Formation of the Al-Khod area, where they mainly found quartzose, red-algal-peloidal-foraminiferal

grainstone. Similar to Nolan et al. [1] they noticed that the basal part of the Seeb Formation is overlain by limestone with nodular bedding. Beavington-Penney et al. [7] interpreted the depositional setting as a low intertidal to shallow subtidal environment, probably backed by mangrove swamps.

Although focusing on the Rusayl Formation, the paper by Dill et al. [17] includes a sedimentary log of the basal part of the Seeb Formation from Al-Khod Village, in which they documented cross-bedded limestone in the lower part and limestone with nodules in the upper part as well as two beds of terra rossa paleosol. Thus, they suggested the upward evolution of the basal part of the Seeb Formation from base to top: (1) intertidal to shallow subtidal and supratidal (terra rossa) to (2) intertidal to supratidal (terra rossa) and again (3) an intertidal to supratidal (paleokarst surface) environment.

Most recently, Hersi and Al-Harthy [8] studied the Seeb Formation in the Al-Khod area and provided a clear regionally applicable subdivision of the formation into five lithofacies “units”, avoiding the formal term “member”. According to their subdivision, the basal Unit 1 is characterized by cross-bedded, sandy, bioclastic packstone to grainstone, which accumulated in a high-energy beach-to-intertidal environment, followed by the limestones of Unit 2, which are indistinctly and nodularly bedded.

Evidently, many data and interpretations have already accumulated on the basal part of the Seeb Formation. Some of the most commonly mentioned characteristics are frequent cross-bedded grain to packstones, which contain benthic foraminifera, green and red algae as well as other bioclasts and occasional nodular bedding in the lowest 30 m of the formation, which is a dominant aspect of Unit 2. The interpretations of the depositional setting, however, differ and include shallow, open, carbonate shelf [1], carbonate ramp [3], a low intertidal to shallow subtidal environment [7], a shallow marine and partly supratidal environment [17], or a beach-to-intertidal setting [8].

The above-mentioned publications do not include specific microfacies studies and related photographic evidence of flora, fauna and textures. Regarding the few reported ones, it is unclear whether they are specifically referring to the basal part of the formation. The only one published photomicrograph of the basal part of the Seeb Formation is from Hersi and Al-Harty [8], showing a bioclastic grainstone with benthic foraminifera (e.g., *Alveolina*), echinoids and red algae. In addition, no published lithostratigraphic logs exist and no correlation attempts have been made to explain the apparent thickness variations of the basal part of the Seeb Formation. Our correlated logs are meant to help define Unit 1 and to show the lateral variation of Unit 1 and where the boundary to the overlying Unit 2 is.

We want to elucidate the microfacies evolution of the basal Unit 1 of the Seeb Formation and its implications with respect to their depositional setting to further improve facies understanding. To do this, we logged four sections bed-by-bed and documented the lithostratigraphic positions of all identified microfacies which we classified according to the standard microfacies (SMF) and facies zones (FZ) system [18] (Flügel, 2010). Since the understanding of the Cenozoic tectonics of the study area has also improved significantly during the past two decades (e.g., regional doming; section Geological Setting Section 2), we correlate lithological observations with regional tectonics, also taking into account the long-term eustatic sea-level curve [19].

2. Geological Setting

The formation of the Oman Mountains was triggered by the late Cretaceous obduction of the Tethys-derived Semail Ophiolite and Tethyan ocean floor sediments of the Hawasina units (Figure 1) when the Tethys Ocean was partly closed (e.g., [20–29]). Mountain building was also associated with the development of large domes, also known as “culminations”, in the newly created mountain belt [review in 29]. Two large culminations are the Jabal Akhdar Dome in the West and the Saih Hatat Dome in the East (Figure 2). Intervening is the smaller Jabal Nakhl area/subdome (for location see Figure 2), whose northern part occurs as the western structural continuation of the Saih Hatat Dome (Figure 2) [30,31].

The Jabal Nakhl Subdome and the Saih Hatat Dome are connected via the Fanjah Saddle (Figure 2) [32].

The regional uplift history has been studied by Poupeau et al. [33], Saddiqi et al. [34], Grobe et al. [35,36] and Hansman et al. [37]. Differential Cenozoic exhumation and doming have been established for the Saih Hatat and Jabal Akhdar domes [37]. The Saih Hatat Dome was exhumed relatively quickly from the late Cretaceous until the early Eocene (50 Ma) and then relatively slowly (decreased doming) and evenly, while the Jabal Akhdar Dome was heating up (no doming) until 44 Ma and then cooled relatively fast (doming and exhumation) until 34 Ma (Hansman et al. [37]). Based on the distribution of the post-tectonic and partly terrestrial Al-Khod and Qalah formations, Coffield [32] concluded that the culminations on both sides of the Fanjah Saddle (Saih Hatat Dome and northern part of the Jabal Nakhl Subdome) initially emerged during the same deformation phase.

Both main domes, including the Jabal Nakhl Subdome, are flanked in the North by a major extensional fault, the Frontal Range Fault (Figure 2), which was active from the late Cretaceous to the early Eocene (first faulting interval) and during the late Lutetian to Oligocene (second faulting interval) due to gravitational collapse of the Oman Mountains [12,38]. The four studied sections are located north of both domes.

Overall, the Permo-Mesozoic stratigraphy is dominated by shallow marine carbonates, which accumulated on the Arabian platform (Figure 1). The respective formations are grouped together as the “Hajar Supergroup” (Figure 1), which is 2 km thick [6]. Most of the formations are limestones. Notable exceptions are the Permo-Triassic Saiq and Mahil formations, which are mainly represented by dolostones and the Jurassic Mafraq Formation, which is dominated by limestone but also includes siliciclastic deposits. The marine platform development halted in the course of the ophiolite obduction causing the formation of the Aruma Foreland Basin, in which the Muti and Fiqa formations of the Aruma Group accumulated (Figure 1).

Following obduction, the post-tectonic, siliciclastic, intramontane Campanian (?) to Maastrichtian? Al-Khod Formation (lateral equivalent Qalah Formation) was deposited, nonconformably overlying the ophiolite [1,9,39] (Figure 1). Above an angular unconformity, shallow marine conditions resumed from the Paleocene to Miocene (Pliocene?), dominated by limestone deposition [1–3,10,17,40–46], including the Seeb Formation [7,8,16] (Figure 1). Among the Cenozoic formations depicted in Figure 1, the Rusayl and Barzaman formations contain, besides limestones, also notable amounts of siliciclastic sediments, marl and sandstone as well as shale, sandstone and conglomerate, respectively.

During the Cenozoic, overall stable depositional conditions existed [15] at a time of slow but causally unspecified slow subsidence [33]. The Seeb Formation of the study area accumulated north of the Oman Mountains (Figures 1, 3 and 12 of [1]).

From 55 to 39 Ma, the long-term eustatic sea-level curve indicates a steady rise [19]. However, the Seeb Formation is known for the lack of evidence for sea-level changes [7].

While the early Eocene is known for its very warm global climate ([47]; Paleocene-Eocene Thermal Maximum, [48]; Early Eocene Climatic Optimum, [49]), the middle Eocene climate seems to have cooled [50], although a global warming event during the middle Eocene Climatic Optimum, MECO, occurred (e.g., [51–53]).

At least, since the uppermost Cretaceous, the Oman Mountains existed, and marginally to the mountains, the Jafnayn, Rusayl and Seeb formations accumulated (Nolan et al., 1990). The region was affected by post-“mid”-Eocene deformation related to the Arabia–India convergence [14,54] as expressed by the deformation of the “Tertiary Ridge” (Figure 3) [55], representing our study area. Deformation of the “Tertiary Ridge” is characterized by WNW-directed, left-lateral shearing deforming Paleogene formations (Figure 1), which are best exposed in three hogbacks (inclined strata-forming ridges). The southeastern hogback is made up of the limestones of the Jafnayn Formation, the middle one by Member 2 of the Rusayl Formation, also represented by limestones and a northeastern hogback that is formed by the limestones of the Seeb Formation. Tilting of the strata is less pronounced to the SE, making the hogbacks more widely spaced in this direction.

3. Methods

Four sections were analyzed for this study (Figure 3) representing the basal part of the Seeb Formation (Unit 1) *sensu* Hersi and Al-Harthy [8], which account for a cumulative thickness of ~103.5 m.

From these sections, we collected 57 samples for microfacies analysis, corresponding to ~1 sample per 1.8 m. We studied the microfacies of the thin-section samples following Flügel's [18] extensive concept of standard microfacies (SMFs) and facies zones (FZs) for shallow marine limestones, which has recently been tabulated [56] for practicality. Using this method, observed SMFs can directly be linked to particular FZs, which provide details of the depositional environment. Not all shallow marine limestone samples match an SMF. Our intention was to find matches in our samples with SMFs to constrain the depositional setting via FZs. Using the SMF/FZ method keeps facies descriptions and interpretations brief and concise.

To determine mineral compositions for comparison of two samples from Unit 1 and one sample from the subjacent Rusayl Formation, we analyzed them by powder X-ray diffraction (XRD) using an X'pert Pro X-ray machine (Panalytical).

The observed foraminifera were used to date Unit 1. In addition, three more thin-sections were made to study gutter casts in detail that do not occur in one of the measured sections. In our descriptions of the different outcrops/sections, we proceed from west to east.

4. Results

We present the studied sections from the NW to the SE, covering a distance of 8.3 km. Within the study area, the Seeb Formation dips between 24 and 90° towards the NNE.

Sections 1 and 2 consist mainly of grainstones and packstones, which are represented in the same way in the logs as a distinction is not always clear. The microscopic analyses show that grainstones are more common than packstones and that the textural changes are gradual or associated with alternating laminae, which include the two textures. In thin-sections, we observed that particle sizes in some grainstones may increase locally so that the term "rudstone" would be applicable, and at the same time, we observed that coarse foraminiferal grainstones may locally blend into a finer-grained peloidal grainstone. Fluctuations in water energy and sediment transport may cause the formation of sedimentary layers (laminae in the present case) differing in depositional texture, constituent composition, grain size and grain packing ([18], p. 714). The depositional texture and composition of bedded limestones may vary within the scale of millimeters and a few centimeters ([18], p. 716).

Among bioclasts, benthic foraminifera and echinoids are common. Dasycladacean green algae as well as red algae are less common. Bivalves, gastropods and ostracods are relatively rare. Corals and byozoans occur even more scarcely. The foraminifera commonly show signs of reworking.

4.1. Section 1

Section 1 is the northwesternmost section. This natural outcrop is located 80 m NW of Wadi Al-Khod ("arrow 1" in Figure 3; coordinates 23°34'40.36" N/58°7'9.03" E). The outcrop surface of the inclined beds is basically horizontal, except for some beds which represent meter-high ridges (small hogbacks). In this section, Unit 1 is at least 21.5 m thick. The lower contact to the Rusayl Formation is not exposed, while the upper contact to Unit 2 of the Seeb Formation is very well exposed, characterized by an abrupt change from regular to nodular bedding of Unit 2 as described by Nolan et al. [1], Beavington-Penney et al. [6] and Hersi and Al-Harthy [8]. The contact shows neither erosion nor a hardground. The beginning of nodular bedding readily identifies the contact between Units 1 and 2 in the field.

The limestones are gray and weather in hues of yellow as in all other sections. The bedding is thick to very thick. The limestone beds contain a small percentage of detrital

quartz and display soft sediment deformation involving slump folds (Figure 4A), especially in the lower part of Unit 1. Other sedimentary structures are curved cross-bedding with asymptotic/tangential lower contacts (Figure 4B), herringbone cross-bedding (Figure 4C) and horizontal, parallel lamination. Encrusting red algae, large benthic foraminifera and gastropods can be identified with the naked eye. A boundstone occurs a few centimeters below the base of Unit 2 as a 15 cm thick layer with white patches of encrusting red algae (Figure 4D). These patches are ≤ 15 cm thick and extend a few decimeters laterally at a distance of a few decimeters from one another. This layer can be followed in the field ~ 100 m to the NW where it is covered by scree. The lack of exposure between 10.5 and 14 m in the sedimentary log (Figure 5) is intriguing as Unit 1 usually contains in its upper part a thick shale horizon of little resistance to weathering and erosion.

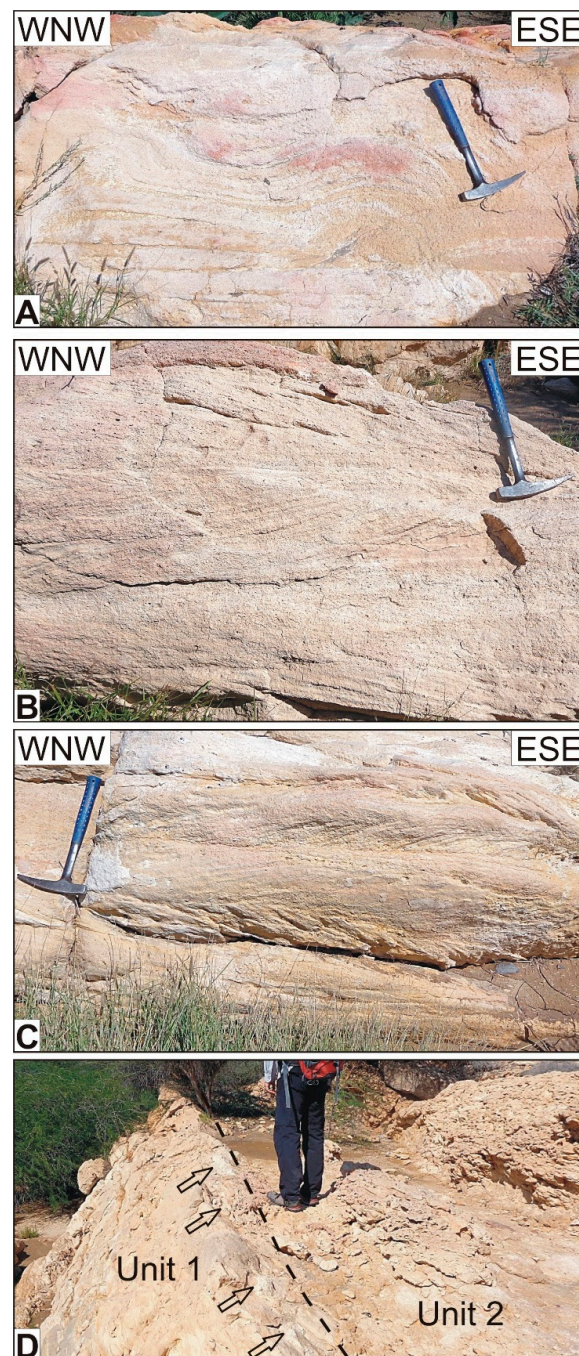


Figure 4. Outcrop photographs of Section 1. (A) Slump fold in the lower part of the section (3 m above base of the section). (B) Sizeable curved cross-bedding near the base of the section (14 m above

base). (C) Herringbone cross-bedding from near the top of the section (15 m above base of the section). (D) Uppermost part of Unit 1 with four white patches of encrusting algae, marked by four arrows. The dashed line marks the boundary between Unit 1 (left) and Unit 2 with nodular bedding (right).

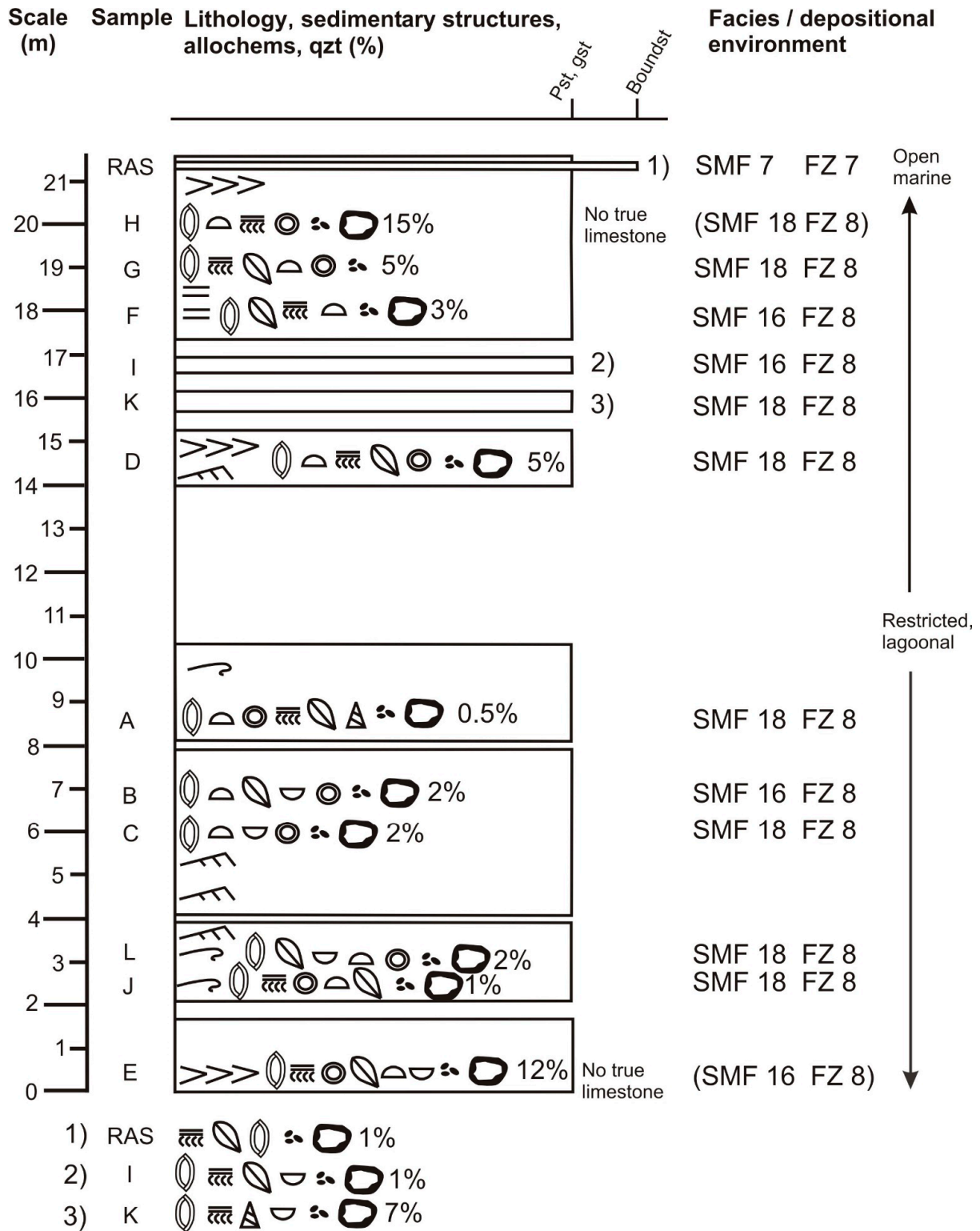


Figure 5. Detailed lithostratigraphic and facies log of Section 1, based on field data and microscopic analyses. Section 1 displays seven gaps of exposure. The frequency of the depicted bioclats decreases

from left to right. The frequency of the portrayed non-skeletal grains also decreases from left to right. Percentages relate to content of detrital quartz. Note that there are three SMF types, mainly representing FZ 8 which is a restricted marine platform interior. SMF 7 represents an open/normal marine platform interior of a rimmed platform. The legend is shown in Figure 6.

Legend



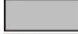

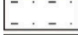



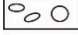












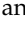
	Limestone		Bivalve
	Dolostone		Bryozoa
	Shale		Coral
	Sandstone		Dasycladacean
	Conglomerate		Echinoid
	Cross-bedding		Foraminifer, benthic
	Herringbone cross-bedding		Gastropod
	Parallel lamination		Green alga
	Slump		Ostracod
SMF	Standard microfacies		Red alga
FZ	Facies zone		Bioturbation, unspecified
			Cortoids
			Peloids

Figure 6. Legend for Figure 5 and the following log figures.

Under the microscope, the samples of Section 1 display a dominance of foraminiferal grainstones/packstones (Figure 7A) over peloidal grainstones/packstones (Figure 7B). The most frequent bioclasts are benthic foraminifera (Figure 7A) and echinoid fragments (Figure 7C). Also present are dasycladaceans, red algae, bivalves, gastropods and ostracods. Among the red algae, branching red algae are the most common. Other allochems are common peloids and some cortoids. Figure 7D depicts an encrusting red alga from the boundstone at the top of Section 1.

The foraminiferal limestones represent SMF 18-FOR and the peloidal limestones SMF 16 [18]. The boundstone, close to the top of Section 1, represents SMF 7 [18].

All samples display detrital quartz grains. In samples E and H, the quartz content exceeds 10%. These samples are considered “quartz arenitic limestones” and, thus, no true limestones. Detrital quartz may occur at any level of Section 1 (Figure 5; Table A1 of Appendix A).

4.2. Gutter Cast Outcrop

Gutter casts are down-bulges on the bottom of a sedimentary bed and are of great length (usually ≥ 1 m) compared with its width and depth (a few to several decimeters). In cross-sections, they have the form of small channels [57] and may be U- or V-shaped [58]. Gutter casts are common in shallow marine sediments, where they are attributed to fluid scour, in many cases by storm currents [59].

Between Sections 1 and 2, within the northeastern hogback (outcrop “GC” in Figures 3 and 8; coordinates 23°34′29.46″ N/58°7′29.35″ E), the basal bed of Unit 1 exposes abundant gutter casts which locally cover a part of the basal bedding surface (Figure 8A,B). Internally, the gutter casts exhibit parallel lamination and lack of bioturbation and macroscopically they lack deformation other than tilting. Based on orientation, two sets of gutter casts can be distinguished (Figure 8A). Most gutter casts (Set 1) dip with 20 to 40° to the SE and are a few to several decimeters wide and a few decimeters deep while the remaining ones (Set 2) are fewer, vertical and measure a few decimeters in width and depth (Figure 8B). Some gutter casts change direction from that of one set to that of the other. It cannot be determined whether one set is systematically older. Back-rotated, the gutter casts of Set 1 trend paleogeographically ~E-W while the gutter casts of Set 2 trend ~SW-NE.

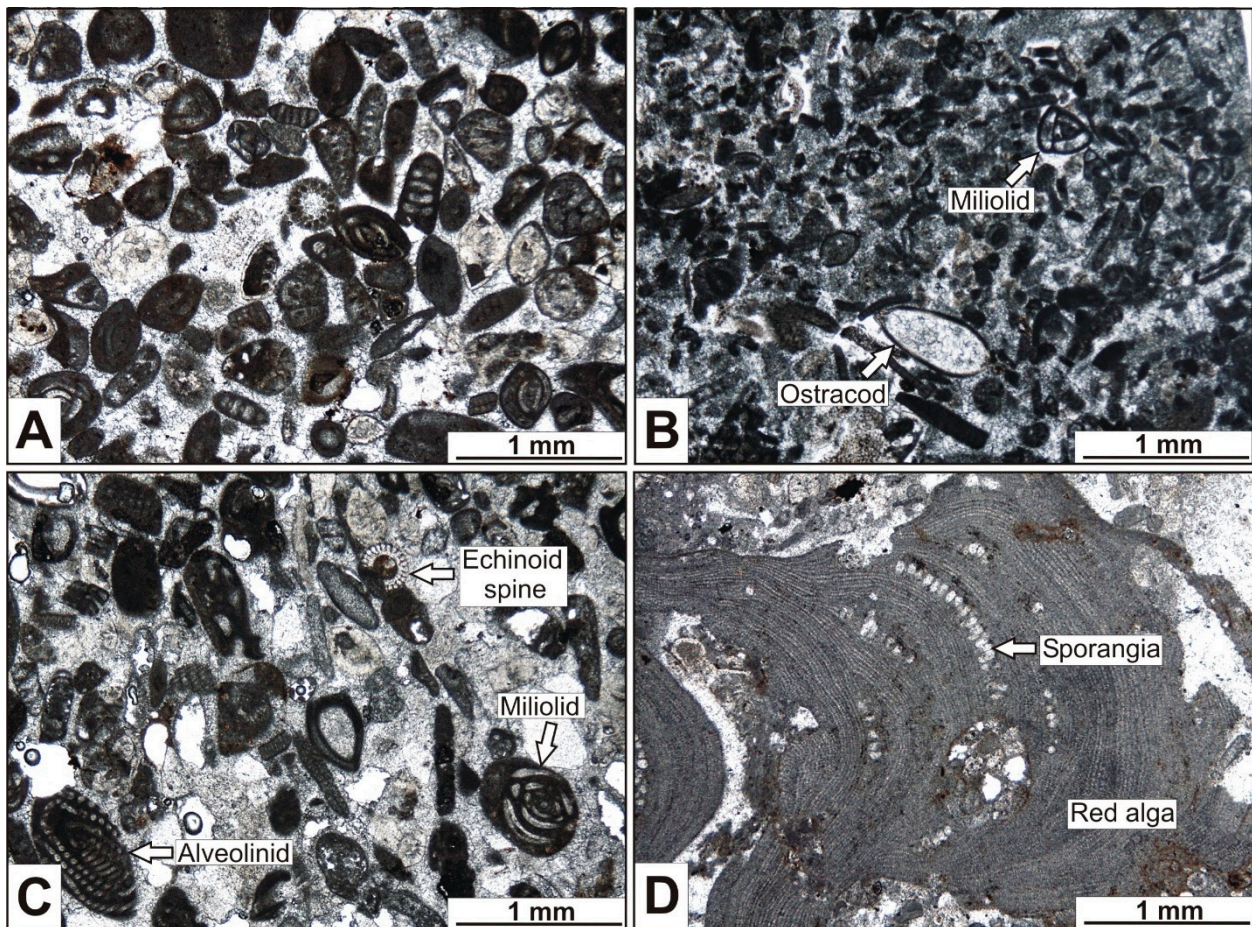


Figure 7. Microphotographs of Section 1 (all PPL). (A) Foraminiferal grainstone representing SMF 18-FOR. Most foraminifera have a micritic-walled test. The round bioclast in the center is a dasycladacean green alga. The bioclasts are accompanied by peloids and cortoids. Sample J. (B) Peloidal grainstone representing SMF 16-NON-LAMINATED. Besides peloids, a cement-filled, thin- and smooth-walled ostracod with recurved valves and a miliolid are shown. Sample I. (C) Foraminiferal grainstone with benthic foraminifera (alveolinid and miliolid) and echinoid fragment (spine and transverse section) as the most abundant bioclasts of Section 1. Note reworking (abrasion) of alveolinid! SMF 18-FOR. Sample D. (D) Boundstone with encrusting red algae from the top of Section 1, representing SMF 7. The alga displays sporangia. Sample RAS.

Internally, three thin-section samples of the gutter casts confirm the presence of parallel lamination and the absence of bioturbation. There is also no microscopic evidence of fecal pellets. Two samples contain ~20% well-sorted angular to subrounded fine quartz sand and a few small benthic foraminifera. One sample is slightly coarser than the others. It lacks bioclasts and contains 40% angular to subrounded fine to medium quartz sand.

4.3. Section 2

Section 2 is located 1 km to the SE of Section 1. This excellent outcrop is situated along the western side of the road that leads into Al-Khod Village from the North (“arrow 2” in Figures 3 and 9; coordinates 23°34′23.79″ N/58°07′42.04″ E). The thickness of Unit 1 in this location is 24.2 m (Figures 9 and 10). The basal contact to the shale-bearing Rusayl Formation is well exposed as is the upper contact to Unit 2 of the Seeb Formation with the dominant nodular bedding style (Figure 9). Both contacts are readily identified in the field.

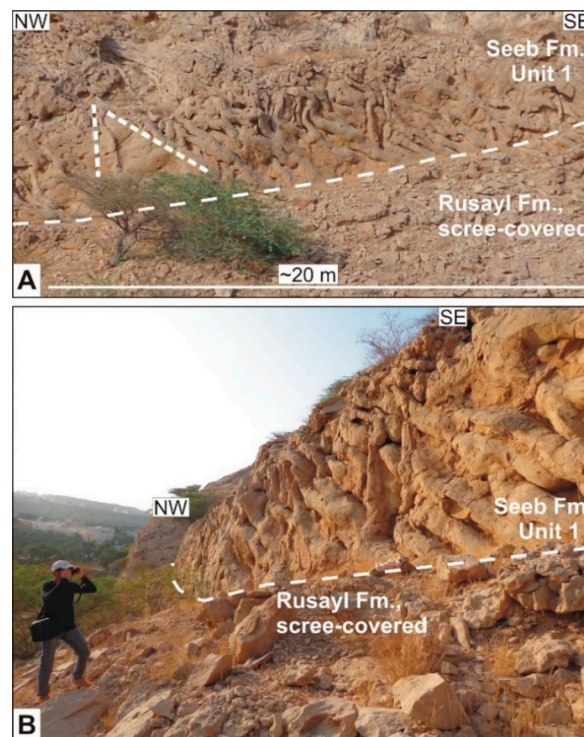


Figure 8. Abundant gutter casts associated with the lower bedding plane of the basal bed of Unit 1 between sections 1 and 2. (A) Frontal and distant view, showing the great number of closely spaced gutter casts. The gutter casts form two differently oriented sets, which are indicated by the two short, dashed lines. (B) Oblique close-up view of the gutter casts from the subvertical basal bed of Unit 1.

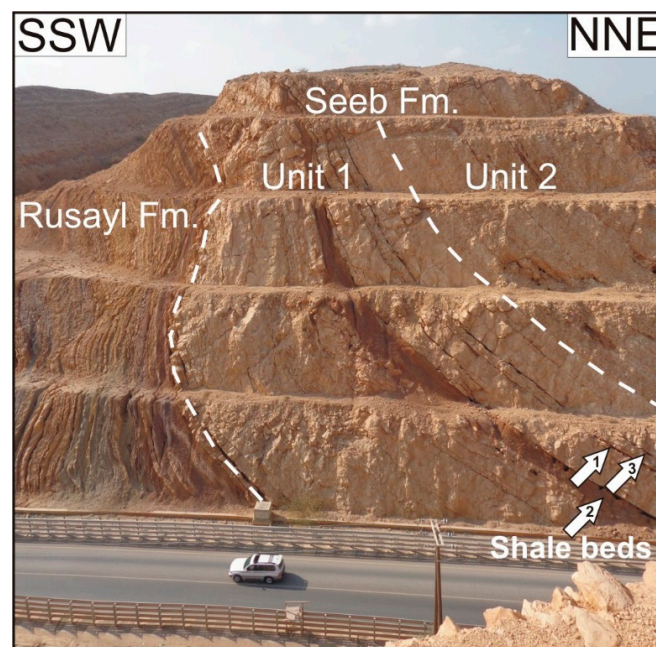


Figure 9. Section 2. Unit 1 between the subjacent Rusayl Formation and the overlying Unit 2. The uppermost part of the Rusayl Formation has been interpreted as terra rossa [17]. This outcrop exposes one thick and two thin shale beds in Unit 1. Arrows 1 and 2 indicate the terra rossa beds *sensu* Dill et al. [17]. Arrow 3 points to a shale bed, indistinguishable from the terra rossa beds, which was not referred to by Dill et al. [17]. The beds of Unit 2 are characterized by nodular, bioturbated limestone [7]. In the upper part of the outcrop, the thickness of the lowest part of the Seeb Formation appears to be lower. This is due to extensional faulting (Figure 5 of [55]). Note the changing dip angle of Unit 1! Road north of Al-Khod Village.

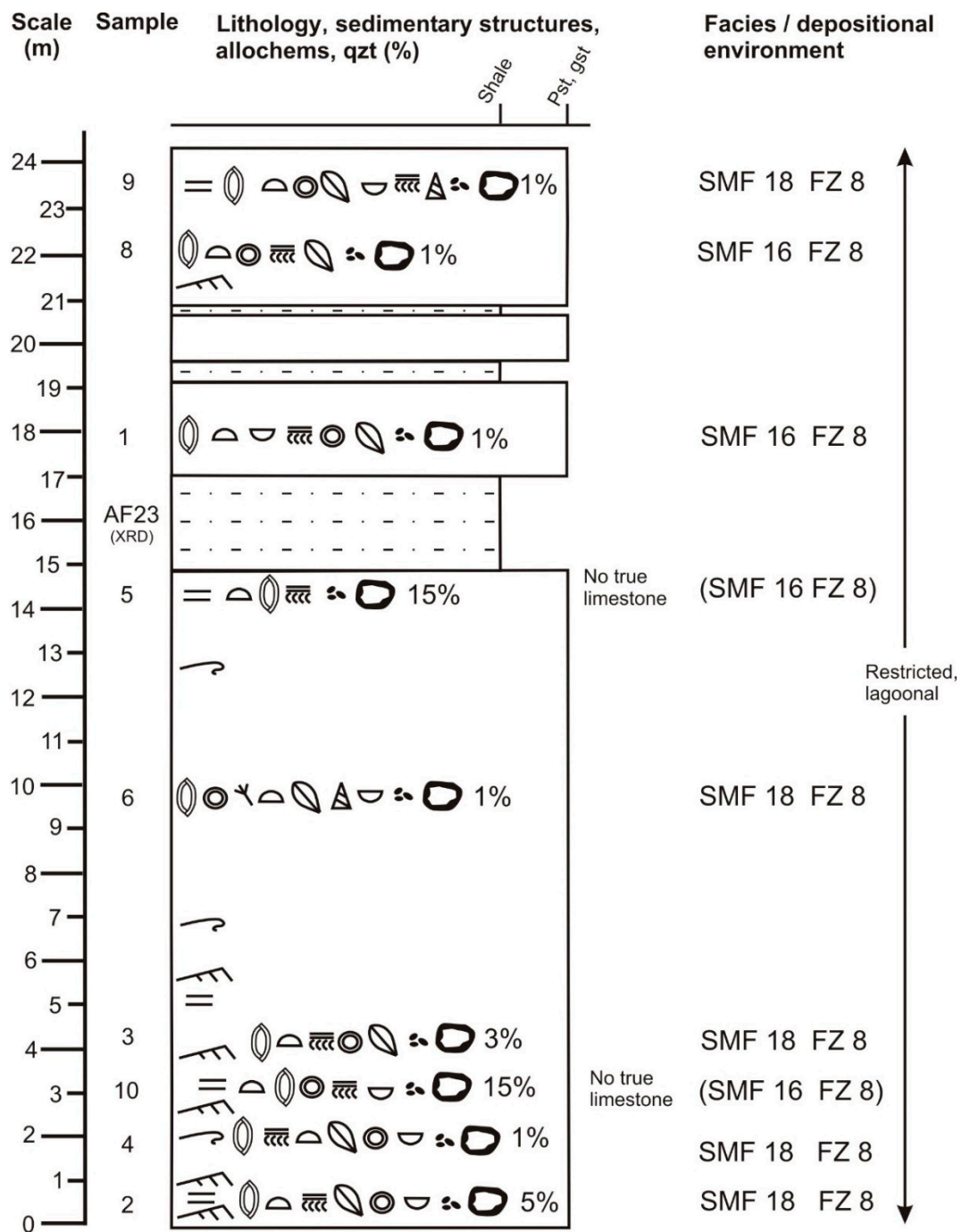


Figure 10. Detailed lithostratigraphic and facies log of Section 2, based on field data and microscopic analyses. Frequency of bioclasts decreases from left to right. Frequency of other allochems also decreases from left to right. Percentages relate to content of detrital quartz. The shale beds at 16 and 19 m above base have been interpreted as terra rossa by Dill et al. [17]. Note that there are only two SMF types! Both represent FZ 8 which is a restricted marine platform interior. The legend is shown in Figure 6.

The section is characterized by thick- to very thick-bedded limestones, comprising a small percentage of detrital quartz grains. The limestones display curved cross-bedding with asymptotic/tangential lower contacts, horizontal, parallel lamination and soft-sediment deformation with slump folds. Larger benthic foraminifera and rare gastropods can be identified with the naked eye.

In addition to the limestones, there are three intercalations of shale in the upper part of the section, the thickest one measuring 2.2 m (Figures 9 and 10). Two of those intercalations have been interpreted as terra rossa paleosols by Dill et al. (2007). This interpretation is based on apparent similarities with deposits in the upper Rusayl Formation which show the presence of quartz, smectite and kaolinite (Dill et al., 2007). The terra rossa beds are supposed to have originated from weathering of calcareous bedrocks (Dill et al., 2007) although a number of researchers had demonstrated that calcareous bedrocks alone could not have produced paleosols of such thicknesses (Dill et al., 2007 and sources therein). The interpretation is also surprising as no hematite or goethite were reported by Dill et al. (2007). The thickest intercalation in Unit 1 is largely brown but also displays a purple hue in the middle of the bed. Such slightly purplish sediments may display veins filled with secondary gypsum in different levels of the Rusayl Formation. We sampled the purplish material for XRD analysis. The main result of Sample AF23 is shown in Table 1 and indicates the presence of kaolinite and quartz but neither hematite nor goethite. The complete XRD analysis of Sample AF19 is documented in Appendix E. Microfossils are also absent in Sample AF23.

Table 1. XRD Analyses of shales from the study area.

Mineral	Formula	Wt%
A. Thickest shale bed of Section 2 (Seeb Formation, Sample AF23).		
Quartz	SiO ₂	30
Kaolinite	Al ₂ Si ₂ O ₅ (OH) ₄	70
B. Shale bed of Section 4 (Seeb Formation, Sample AF19).		
Quartz	SiO ₂	30
Gypsum	CaSO ₄ ·2H ₂ O	45
Kaolinite	Al ₂ Si ₂ O ₅ (OH) ₄	25
C. Purplish shale bed from the top of the Rusayl Formation of Section 2 (Sample AF24).		
Quartz	SiO ₂	40
Kaolinite	Al ₂ Si ₂ O ₅ (OH) ₄	60

Our microscopic observations of Section 2 are compiled in Table A2 of Appendix B. Section 2 is dominated by foraminiferal grainstones/packstones and peloidal grainstones/packstones with the former being slightly more common than the latter. The limestones frequently include benthic foraminifera and echinoid fragments and less frequently red algae, dasycladaceans, gastropods, bivalves and ostracods. Other allochems are abundant peloids and common cortoids. The foraminiferal grainstones/packstones and peloidal grainstones/packstones correspond to SMF 18-FOR and SMF 16 [18], respectively. The lamination of samples 2 and 9 is distinguished by their micritic or sparitic nature, varying grain size and frequency of bioclasts as well as different amounts of detrital quartz (Figure 11).

All samples contain a small percentage of detrital quartz. Samples 5 and 10 contain >10% of quartz and are, therefore, no true limestones. Detrital quartz may occur at any level of Section 1 (Figure 5; Table A2 of Appendix B).

4.4. Section 3

Section 3 is located 4 km to the SE of Section 2 and 2.4 km south of the campus of Sultan Qaboos University. Section 3 is a natural outcrop on a SW-facing slope of a hogback exposing the Rusayl and Seeb formations (arrow 3 in Figure 3; coordinates 23°33′36.34″ N/58°09′50.43″ E). The thickness of Unit 1 here measures almost 29 m.

Section 3 is characterized by thick- to very thick-bedded limestone (Figure 12) containing a small percentage of detrital quartz grains (Figure 12). Cross-bedding, which is gently curved with asymptotic basal contacts, is relatively rare, while parallel lamination is common (Figure 12). Large benthic foraminifera and gastropods can be identified with the naked eye. Between 12 and 14.5 m is a relatively coarse quartz-bearing limestone.

Besides the limestones, there is also a dolomitized level between 16.5 and 18.5 m. The lack of exposure (scree) in the upper part of the section, between 21.5 and 24 m in the log (Figure 12), is interesting as Unit 1 features a thick and easily erodible shale horizon in its upper part as recorded in the upper parts of sections 2 and 4. At the same time, a similar lack of exposure of such a possible shale level as seen in the log of Section 3 occurs between 10 and 14 m and in Section 1 (Figure 5).

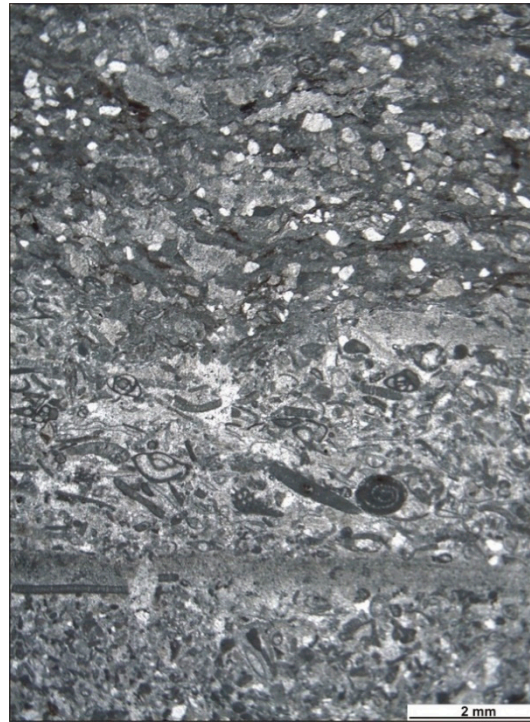


Figure 11. Laminated foraminiferal grain to packstone of Section 2. While the lower half of the microphotograph represents the lamina of a grainstone and sparite with large and frequent bioclasts and limited detrital quartz grains, the upper half is a lamina of a packstone and micrite with small and few bioclasts but frequent detrital quartz grains. Overall, the sample represents SMF 18-FOR. Sample 2. PPL.

Microscopic details of Section 3 are documented in Table A3 of Appendix C. The section is characterized by foraminiferal grainstones dominating peloidal grainstones. Benthic foraminifera and echinoid fragments are the most common bioclasts, followed by less common dasycladaceans, red algae, bivalves, gastropods, ostracods, poritid corals and bryozoans. Peloids are abundant and more common than cortoids. The foraminiferal and peloidal grainstones represent SMF 18-FOR and SMF 16 [18], respectively. Among ostracods, we found relatively thick-walled, benthic types (Figure 13A). Sample S2 features a small partly crushed echinoid test (Figure 13B). One rare coral was found in the coarse-grained part of Sample 5 associated with large benthic foraminifera and quartzite grains (Figure 13C). A quartz-foraminiferal rudstone (“rudstone”, if high detrital quartz content would not be considered; no SMF match) with abundant dark, micritic-walled benthic foraminifera is depicted in Figure 13D. It shows that the bioclasts are embedded in displacive sparry calcite cement (Sample S16).

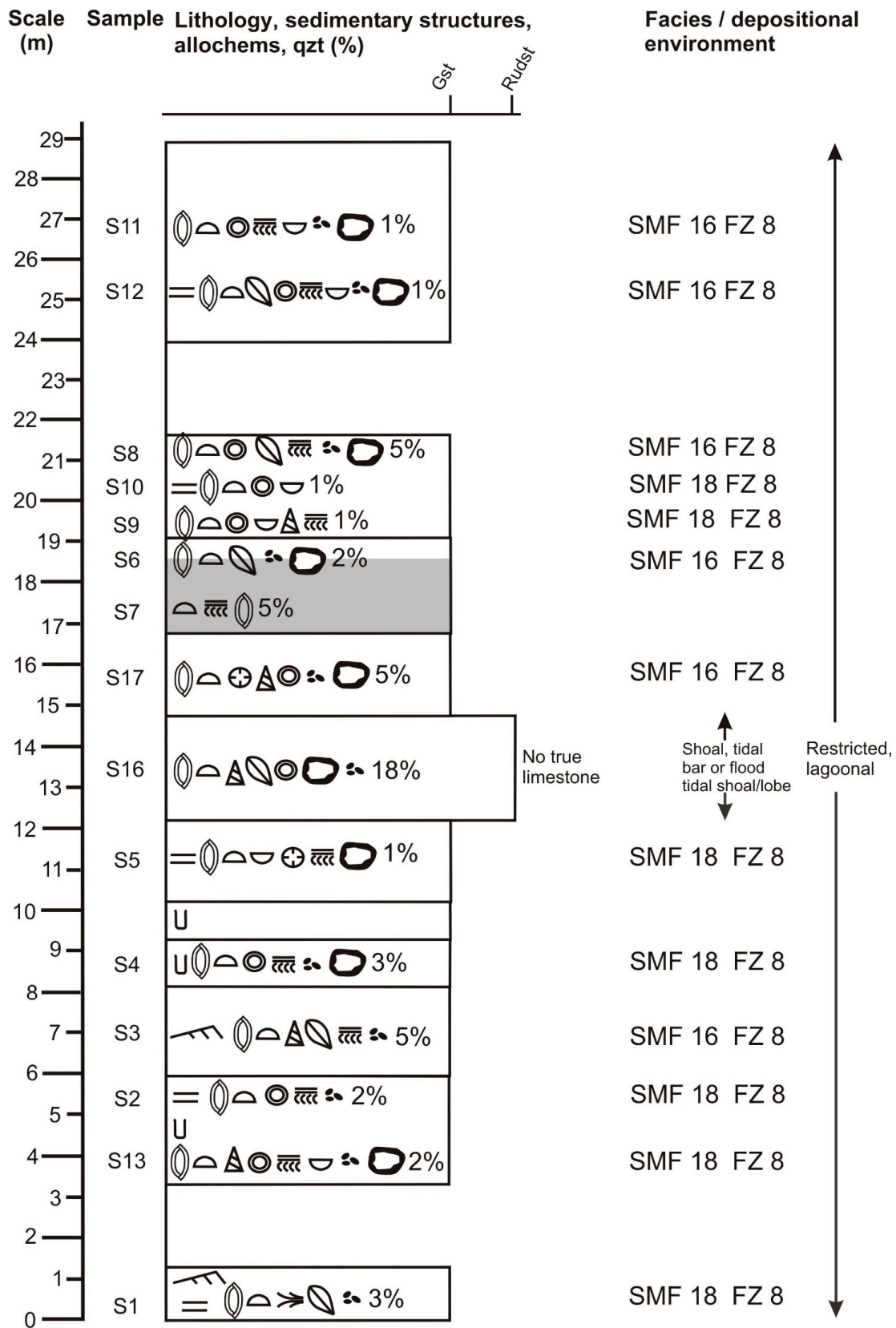


Figure 12. Detailed lithostratigraphic and facies log of Section 3, based on the field data and microscopic analyses. Frequency of bioclasts decreases from left to right. Frequency of other allochems also decreases from left to right. Percentages relate to content of detrital quartz. There are only two SMF types. Both represent FZ 8 which is a restricted marine platform interior. The legend is shown in Figure 6.

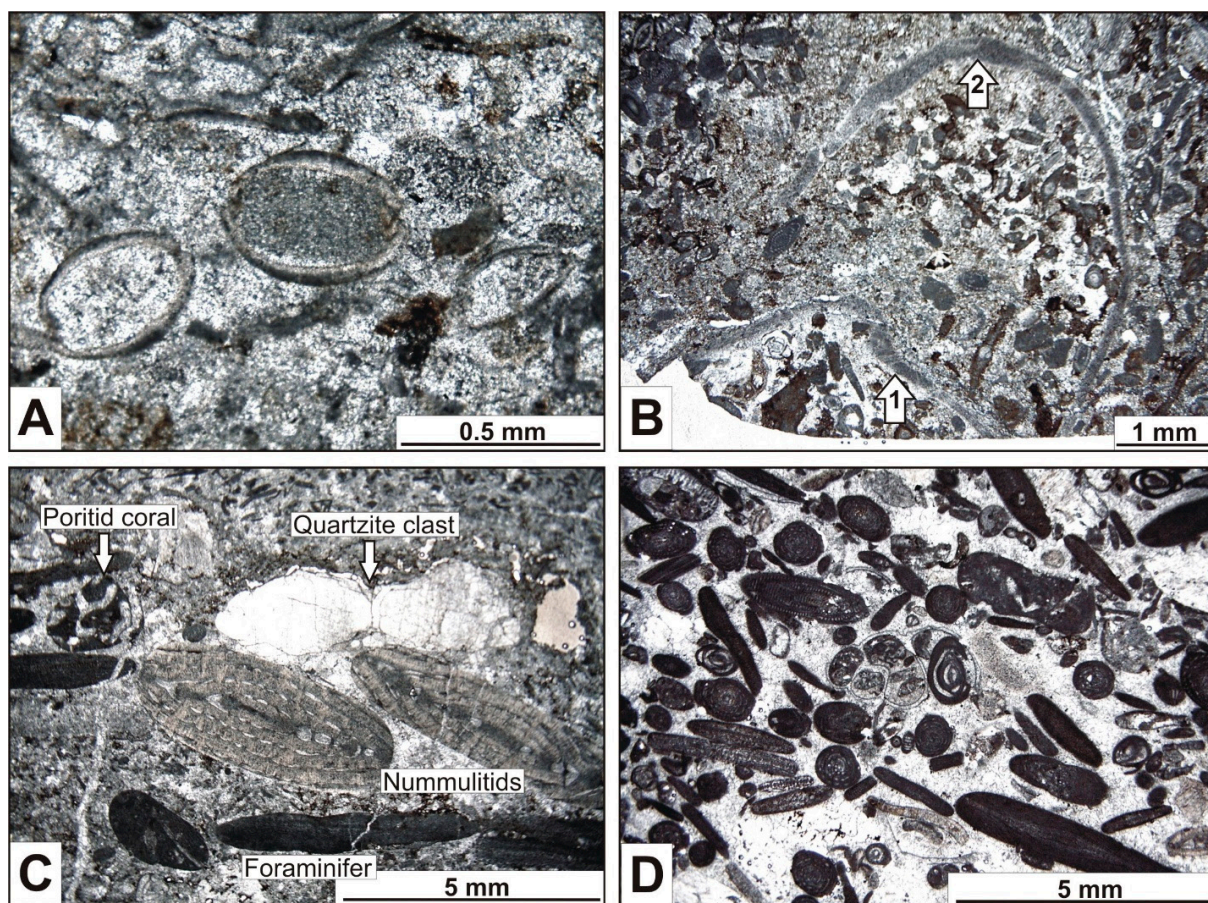


Figure 13. Microphotographs of Section 3 (all PPL). (A) Laminated foraminiferal grainstone from the base of the section with ostracods. The ostracod in the center displays relatively thick-walled valves. The sample is assigned to SMF 18-FOR. Sample S1. (B) Foraminiferal grainstone to rudstone with a small, crushed echinoid test. Arrow 1 marks the flat, basal part of the test while arrow 2 indicates the curved upper part of the test. The lower part became detached from the rest of the test. The sample corresponds to SMF 18-FOR. Sample S2. (C) Foraminiferal grainstone to rudstone, representing SMF 18-FOR. Poritid coral associated with quartzite clast and larger benthic foraminifera (two nummulitids in the center) in the coarse-grained part of Sample S5. Note reworking (abrasion) of the nummulitid on the right! (D) Quartz-foraminiferal rudstone (“rudstone”, if high detrital quartz content would not be considered; no SMF match) with abundant dark, micritic-walled benthic foraminifera. In the center is a gastropod, partly filled with a reworked (abraded) benthic foraminifer. Bioclasts are embedded in displacive sparry calcite cement. Sample S16.

The dolostone is a dolosparite, showing relict bioclasts that survived dolomitization, such as echinoderm fragments as well as micritic-walled red algae and possible micritic-walled foraminifera.

The limestones, again, contain detrital quartz. The coarse-grained limestone between 12 and 14.5 m above the base contains >10% of quartz fragments. If the high quartz content of 18% would not be considered, this would be classified as a foraminiferal rudstone. Detrital quartz may occur at any level of Section 1 (Figure 12; Table A3 of Appendix C).

4.5. Section 4

The southeasternmost Section 4 is located 3.2 km SE of Section 3 along the eastern side of Nizwa Express Road (“arrow 4” in Figures 3 and 14A,B; coordinates 23°22′53.9″ N/58°11′35.4″ E). This high roadside outcrop was newly created thanks to road-widening works. Thus, we had access to fresh outcrops along a pipeline trench and five artificial terraces. The outcrop displays tilted beds, displaced by mostly extensional faults of minor

displacement of ≤ 3 m (Figure 14A,B), but the tilting of the beds and the presence of the terraces allowed us to piece the entire section together from small sections which were logged between and correlated across the faults. While the lower contact with the Rusayl Formation is exposed (Figure 14B,C), the upper contact with Unit 2 is covered by scree (Figure 14A). The thickness of Unit 1 measures ≤ 39.5 m, representing the greatest thickness of all the measured sections.

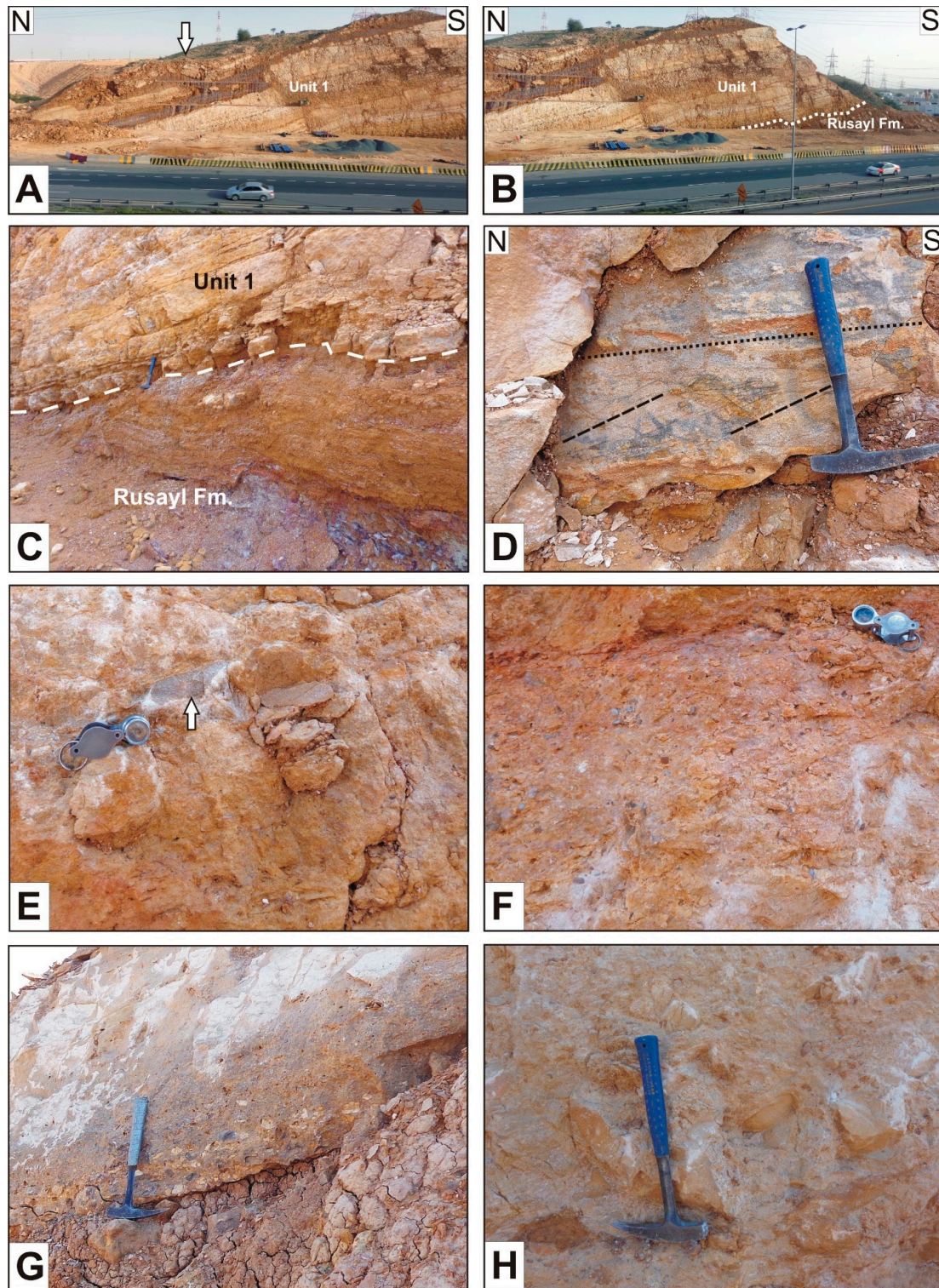


Figure 14. Section 4. (A) Northern and central parts of the outcrop show the shale horizon in the upper part of the section. The pipeline trench is below the road level. Note that shale intruded and

tilted overlying beds (arrow)! (B) Central and southern outcrop segment with exposed contact to the underlying Rusayl Formation. (C) Well-exposed abrupt contact between the Rusayl Formation and Unit 1 (base of section). Note the presence of purplish shale in the Rusayl Formation (bottom right), which contains veins with secondary gypsum! The purplish shale always occurs in the middle of the shale bed. (D) Tabular cross-bedding from the middle of Section 4 (21 m above base). Dotted line indicates orientation of general bedding and dashed line indicates orientation of cross-bedding. (E) Debrite with 6 cm long lithoclast, marked by arrow near the base of the section (3 m above base) (F) Reddish monomictic chert conglomerate from the lower half of the section (12 m above base). (G) Conglomerate directly overlying the shale bed (36 m above base). The light-colored clasts are weathered carbonates. (H) Debrite, representing the coarsest sediment of Unit 1 in all four sections from the top of the section (38 m above base).

Section 4 is dominated by a thick to very thick bedding style. The limestones may contain detrital quartz grains. Cross-bedding (Figure 14D) is as rare as in Section 3, while parallel lamination is common. Larger benthic foraminifera (flat, disk-like nummulites), bivalves and red algae can be identified with the naked eye.

Section 4 differs from the other sections by the presence of a sandstone bed and conglomerates. At 2 to 4.5 m above the base, a debrite occurs with limestone lithoclasts measuring up to 10 cm. The matrix-supported clasts are subangular to subrounded (Figure 14E).

At 12 m above the base is a reddish monomictic granule-to-fine pebble chert conglomerate, sourced from cherts of the Hawasina units. The conglomerate is rich in chert and carbonate sand. The chert clasts are subrounded to rounded and matrix-supported (Figure 14F). The bed cuts down by 15 cm.

About 21 m above the base, a thin, 5 to 10 cm thick, porous, poorly cemented quartz-rich sandstone layer occurs. It is the only sandstone bed we found in Unit 1.

A second carbonate conglomerate occurs above the shale horizon, either separated from the shale by two limestone beds or in direct contact with the shale. This conglomerate occurs at the basal 5 to 20 cm of a limestone bed. The carbonate clasts measure up to 6 cm, are angular to subrounded and matrix-supported. Some clasts are intensely weathered (Figure 14G).

The uppermost bed contains a conglomerate (debrite) which is very similar to the first one we described. The main differences are the larger size (≤ 30 cm) of the limestone lithoclasts and their greater abundance (Figure 14H). This conglomerate is the coarsest sediment we encountered in Unit 1.

The thick to very thick bedding style, the occurrence of cross-bedding and parallel lamination and the positions of the sandstone and conglomerate beds is documented in the sedimentary log of Figure 15. In the upper part of Section 4, a shale horizon is present (Figure 15), displaying close lithological similarities to the shale horizon of Section 2 and the shales of the underlying Rusayl Formation. It tends to be brown at the base and the top, while the center shows a purple hue. In the outcrop of the pipeline trench, purplish shales feature abundant gypsum veins as in the Rusayl Formation. Gypsum veins in purplish shale are also present in the outcrop of the lowest terrace but less numerous in the other terraces. There are no microfossils in Sample AF19. The XRD Sample AF19 of the purplish shale revealed the presence of gypsum (secondary vein material), quartz and kaolinite (Table 1B) and compares very closely to the XRD Sample AF23 from Section 2 (Table 1A) in terms of quartz and kaolinite content. The complete XRD analysis of sample AF23 is documented in Appendix F. As in Sample AF23, Sample AF 19 contains neither hematite nor goethite.

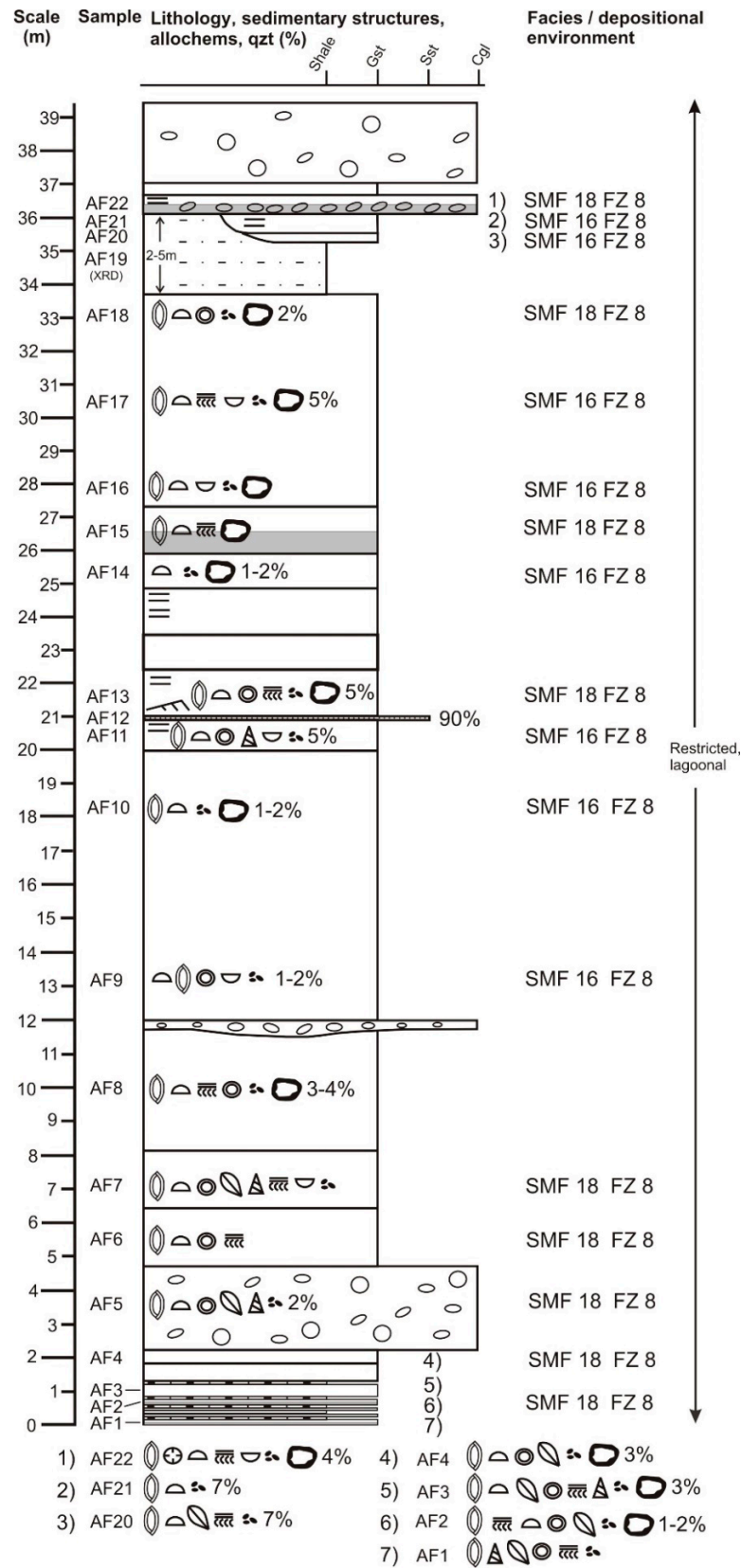


Figure 15. Detailed lithostratigraphic and facies log of Section 4, based on field data and microscopic analyses. Frequency of bioclasts decreases from left to right. Frequency of other allochems also decreases from left to right. Percentages relate to content of detrital quartz. There are only two SMF types. Both represent FZ 8 which is a restricted marine platform interior. The legend is shown in Figure 6.

Because of the lithological similarities between the shale bed in Unit 1 and the shales of the Rusayl Formation, which we observed in the field, we took Sample AF24 from the upper part of the Rusayl Formation (same outcrop as that of Section 2) to compare their mineralogical compositions (Table 1C). The mineralogical similarities are obvious (compare Table 1A,B,C). The complete XRD analysis of sample AF24 is documented in Appendix G.

There is evidence for shale migration in the shape of a shale tongue which is a tabular intrusion of shale that parallels sedimentary rocks [59], positioned above the thick shale bed (Figure 16A,B). Some limestone beds are truncated and dragged where the shale had moved upward into a stratigraphically higher level (Figure 16A,C). Because of this shale intrusion, the primary shale layer is duplicated (Figure 16A). The shale tongue caused tilting of the overlying limestone with a noticeably different dip direction compared to the general bedding attitude. Four limestone boulders became detached as wall rock inclusions and are now “floating” in the shale (Figure 16A,D). The thickness of the shale bed varies between 1.5 and 6 m over short distances in the outcrop. The maximum thickness is associated with a fault, whose kinematic character could not be determined (Figure 16A).

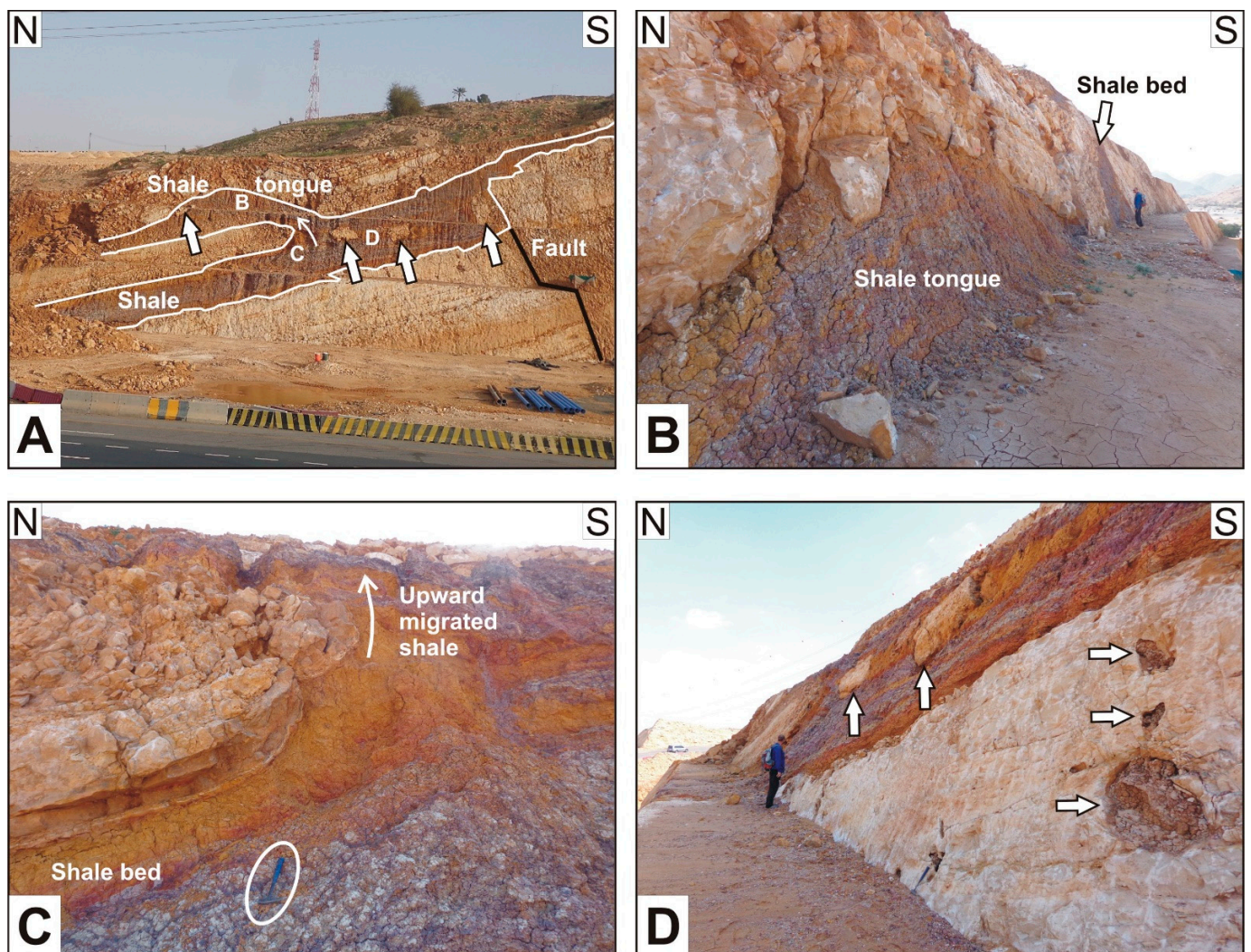


Figure 16. Shale layer of Section 4 and evidence of upward shale migration/intrusion leading to the formation of a shale tongue. (A) Overview of the primary shale bed and the secondary shale tongue. Four detached limestone boulders (arrows) became detached and “float” in the shale. Thickness differences occur over a short distance and may be in part related to faulting. The apparent “kinks” of the fault are due to the fault being exposed at one of the man-made terraces. Note the different dips

of the limestones above the shale tongue! The letters B, C and D mark the sites depicted in B, C and D. **(B)** Upper part of the shale tongue. The shale intrusion caused local SSW dip although the general dip is to the NNE. In the background, the primary shale bed is also exposed. **(C)** This site shows truncation and drag-folded limestone beds due to shale migrating upward into the shale tongue. **(D)** Two detached limestone boulders “floating” in the shale (vertical arrows). Sizeable dissolution features due to karstification filled with reddish residual material (horizontal arrows).

Details of the microscopic analyses are listed in Table A4 of Appendix D. Similar to Section 3, Section 4 is dominated by grainstones. Foraminiferal grainstone samples slightly outnumber peloidal ones. Among the bioclasts, benthic foraminifera are more common than echinoid fragments. Less frequent are remains of red algae, dasycladaceans, ostracods, which are all thinly walled, bivalves and gastropods. We found one coral in one thin-section, while peloids dominate over cortoids. Sample AF6 features a cross-section of a sand dollar (Figure 17A). The coral occurs in Sample AF22, which is partly dolomitized. The coral is poorly preserved. It is associated with relict echinoderm fragments as well as micritic-walled foraminifera and micritic-walled red algae. Sparitic dolomite occurs in Sample AF15 and two thin beds at/near the base (samples AF1 AF2) (Figure 15). The dolostones are sparitic. Seventeen out of the twenty-one thin-sections could be assigned to a specific SMF. Again, the foraminiferal and peloidal grainstones represent SMF 18-FOR and SMF 16 [18], respectively (Figure 15). The content of detrital quartz grains is less than in Section 3. In fact, some limestone beds lack detrital quartz altogether. In all thin sections, the quartz content is $\leq 10\%$ in the limestones, but quartz detritus occurs at various levels of the section. The sandstone bed is a quartz-rich litharenite with 90% of quartz material (Figure 17B,C).

4.6. Foraminifera and Age

Benthic foraminifera are the most common fossils/bioclasts in the limestones of Unit 1 and display a considerable variety, including *Alveolina elliptica*, *Alveolina oblonga*, *Amphistegina* sp., *Assilina* sp., *Astigerina* sp., *Idalina* sp., *Lockhartia* sp., *Linderina rajasthanensis*, miliolids, *Nummulites globulus*, *Nummulites discorbinus*, orbitoids, *Quinqueloculina* sp., *Rotalia* sp., *Rotrobinella* sp., *Somalina dizeri*, *Somalina stefanii*, *Textularia* sp. and *Triloculina* sp. Among them, larger benthic foraminifera are abundant, like those of the *Alveolinidae*, *Nummulitidae*, *Miliolidae* and *Soritidae* families. The most abundant foraminiferal assemblages in all four sections are miliolid assemblages. Besides the miliolid assemblages, we identified other assemblages, including two which provide a middle Eocene age:

1. *Somalina* sp. assemblage with *Somalina stefaninii* [60].
2. *Alveolina* sp. assemblage with *Alveolina elliptica* [61].

Associated with these two assemblages are assemblages which include *Nummulites* sp., *Triloculina*, *Quinqueloculina*, *Pyrgo* and *Idalina*.

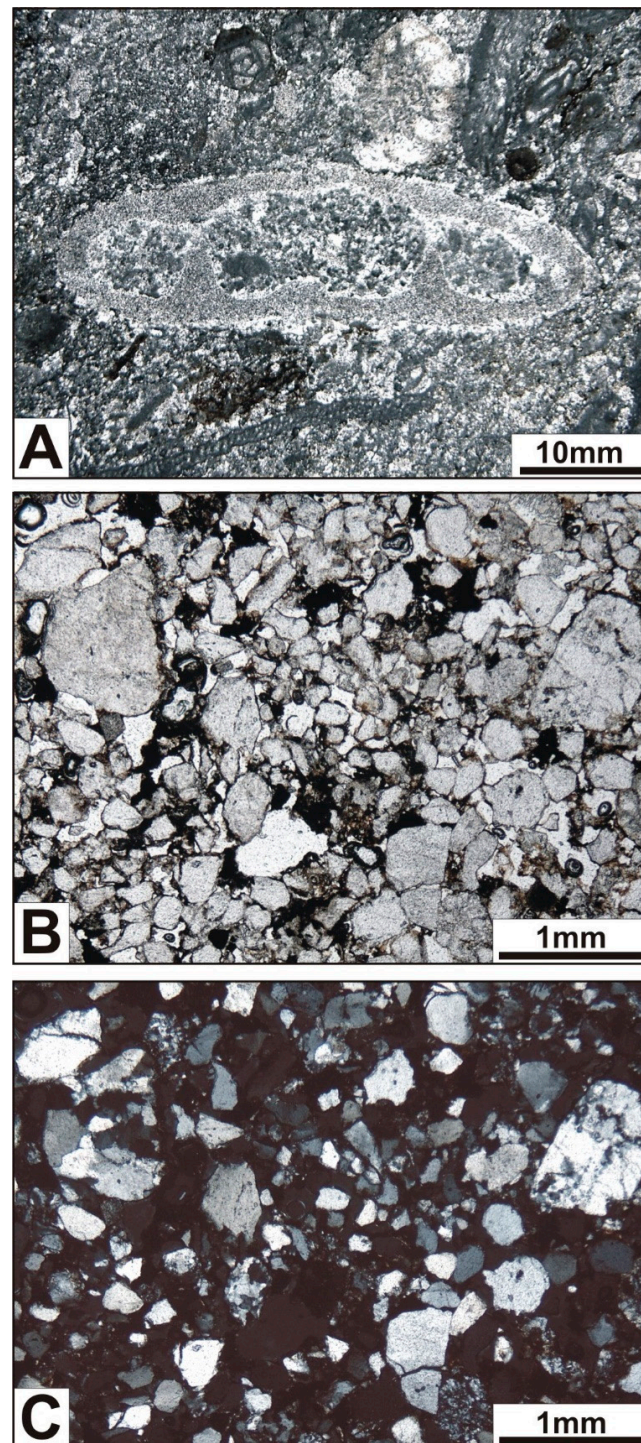


Figure 17. Microphotographs of Section 4. (A) Small echinoid test of a sand dollar in foraminiferal grainstone, assigned to SMF 18-FOR. Sample AF6. PPL. (B) Quartz-rich litharenite with polycrystalline grains of quartzite, muscovite–quartz aggregates, chert and some monocrystalline quartz grains. Note opaque cement! Sample AF12. PPL. (C) Same as in A but XPL.

5. Discussion

5.1. Correlation of Sections

Comparison between the four sedimentary logs of the four analyzed sections reveals that the thickness of Unit 1 increases significantly to the SE (Table 2, Figure 18). The

thickness from Section 1 to Section 4 almost doubles over a distance of 8.3 km (Table 2, Figure 18).

Table 2. Thickness of Unit 1 in the four sections.

Section	Thickness
WSW	
Section 1	>/~21.6 m
Section 2	~24.7 m
Section 3	~28.7 m
Section 4	>39.5 m
ESE	

The base of Unit 1 is exposed in Sections 2 to 4, where the boundary between the subjacent Rusayl Formation and Unit 1 of the Seeb Formation is clearly defined. The top of Unit 1 is well exposed in Sections 1 to 3, where the boundary between Unit 1 and Unit 2 can be easily determined. Therefore, the correlation between the base and top of Unit 1 is unequivocal as depicted in Figure 18.

The thick shale bed in the upper part of Unit 1 is the only marker horizon within Unit 1 and provides the opportunity for a direct correlation. As the shale is weakly resistant to weathering and erosion, the exposure gaps in Sections 1 and 3 are interpreted as the lithostratigraphic positions of the shale bed which has been eroded near the surface (lack of observation; Figure 18). We checked whether some of the six occurrences of beds with >10% detrital quartz could be correlated with one another, but this seems unlikely as no systematic detrital quartz distribution pattern was produced across the logs (Figure 18). However, we point out that all slumps and most detrital quartz deposits of >10% quartz occur below the marker bed (Figure 18). The microfacies analyses of the four sections indicate that the limestones represent the same facies zone across the study area.

5.2. Limestones and Conglomerates

The types of cross-bedding, especially herringbone cross-bedding in Section 1, suggest a depositional environment in line with a tide-influenced setting. In Section 1, SMF 18-FOR and SMF 16 represent the facies zone FZ 8, which is a restricted, lagoonal setting with a water depth below one meter and a few meters to a few tens of meters [18]. This depositional setting could represent a shallow subtidal environment or could have extended to shallow subtidal conditions, as many beds lack cross-bedding, including herringbone cross-bedding. The peloidal grainstones and packstones of SMF 16 signify a lower sedimentation rate compared to that of SMF18-FOR as would exist at quiet sites, allowing for the micritization of allochems [62].

The boundstone (SMF 7), at the top of Section 1, represents facies zone FZ 7 and, thus, normal open marine platform conditions, normally above fair-weather wave base with a water depth of a few meters to tens of meters [18].

Considering the lagoonal environment, the observed dolomitization is tentatively attributed to early diagenesis by occasional seepage-reflux processes (e.g., [63–65]), involving a lagoon setting when high Mg/Ca ratios in the lagoon water were generated by evaporation as deduced for the subjacent Rusayl Formation [45]. Evaporation was favored by restricted conditions. Alternatively, dolomitization may have occurred post-depositionally, coeval with the precipitation of dolomite cement in the late Oligocene to Neogene Barzaman Formation [46].

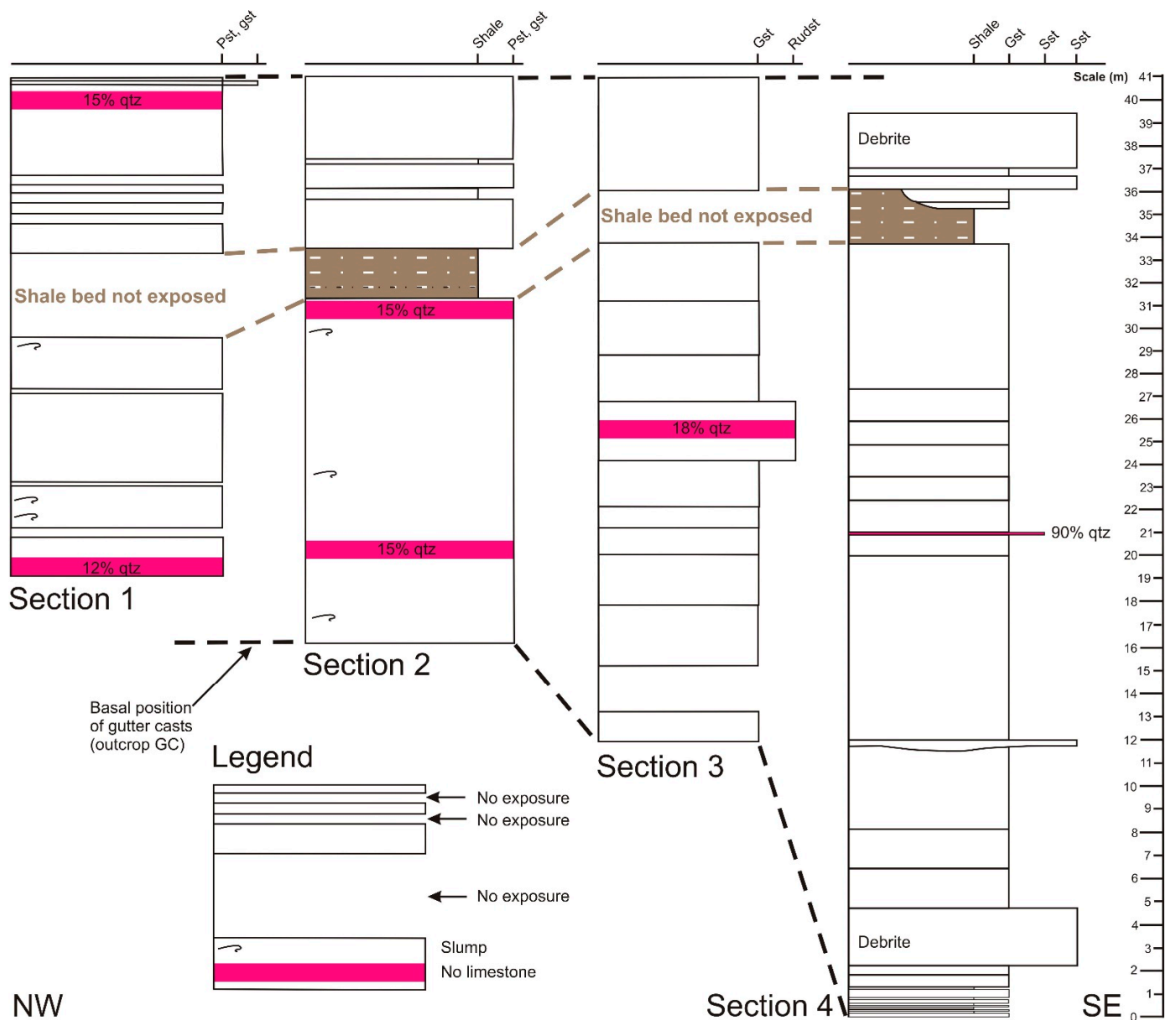


Figure 18. Correlation of the four studied sections. Note the definite correlation between the base of Sections 2, 3 and 4 and the top of Sections 1, 2 and 3! The shale bed in the upper part of Unit 1 is a marker horizon, which has been eroded in Sections 1 and 3. Also, note the thickness increase towards the SE! Beds with a quartz content of >10% are shown in red.

The observed slumps reflect slope instability. Since the Frontal Range Fault was active during the accumulation of the Seeb Formation, seismic tremors could have triggered slumping.

The influx of terrigenous quartz detritus of >10% indicates sporadically increased siliciclastic sediment, shed from the mainland and affecting all sections. The influx of detrital quartz material is greater in the Northwest (Sections 1 and 2) compared to the Southeast (Sections 3 and 4) (Figures 5, 10, 12 and 15 and Tables A1–A4).

The parallel lamination and absence of fecal pellets in the gutter casts rule out an alternative interpretation as large bioturbation (burrows which commonly contain fecal pellets). The gutter casts were the sites of unidirectional flow of storm-triggered suspensions, which created and filled the gutter casts (compare [66]). The parallel lamination indicates that deposition ensued from a laminar state of flow. As we found no evidence for

tempestites in Unit 1, which would have served as evidence for deposition below storm wave base, the gutter casts indicate near-shore formation in a near-shore sediment by-pass zone above fair-weather wave base (Figure 6 of [66]), still relatively close to where the storm suspensions had formed initially. Considering that the Eocene Oman Mountains lay to the South of the study area (Figures 1, 3 and 12 of [1]), the observed gutter casts reflect the presence of a paleoslope with transport to the E and to the NE. We suggest that their presence and high concentration were caused by a changing slope gradient at the onset of deposition of Unit 1.

The depositional environment of Section 2 has been interpreted as a shallow subtidal to intertidal environment with variable energy conditions [17]. A tide-influenced environment would be compatible with the observed types of cross-bedding in Section 2, and some beds that seem to lack cross-bedding may indeed represent a shallow subtidal environment. The presence of SMF 18-FOR and SMF 16 represent the facies zone FZ 8 with the same water depth as deduced for Section 1. If the fine-grained siliciclastic sediments should indeed represent terra rossa paleosols [17], a terrestrial environment would have to be considered, although this seems to be unlikely (see text Sections 4.3 and 5.3). The slumps in Section 2 indicate, again, slope instability.

In Section 3, the standard microfacies are, yet again, SMF 18-FOR and SMF 16 indicating deposition in the facies zone FZ 8 at the same water depth as concluded for sections 1 and 2. The rudstone is the coarsest material in Section 3. We suggest that its coarseness (many large benthic foraminifera, coarse quartz sand and a few quartzite granules) between sediments, indicative of FZ 8, is best explained as a local shoal, tidal bar or flood tidal lobe/shoal, also considering that foraminifer accumulations form shallow banks in the Seeb Formation [16]. Due to the lack of gutter casts, slumps and debrites, the depositional slope of Section 3 appears to have been comparatively stable.

The limestones of Section 4 represent SMF 18-FOR and SMF 16 like the limestones of Section 3. They formed in the same water depth as concluded for Sections 1 to 3.

The debrites (matrix support) indicate the presence of an unstable slope. The other conglomerates (clast support) may represent near-shore deposits. The reddish monomictic granule-to-fine pebble chert conglomerate at 12 m above the base (Section 4), and the litharenite at 21 m above the base (Section 4) may also be near-shore sediments. The sandstone may have formed due to a particular event, like a major discharge event of a river with a nearby estuary. The coarse lithoclasts were shed from the doming areas of the Jabal Akhdar/Jabal Nakhl and the Saih Hatat. With reference to the entire Seeb Formation, Beavington-Penney et al. [7] suggested that particles of quartzose peloidal limestones may have been moved as longshore drift.

5.3. Shale Bed

The gypsum in the shale is secondary as it occurs only in veins. In the Rusayl Formation, gypsum veins are strikingly abundant, including veins that are a few centimeters wide. The Rusayl Formation also contains shale with a notable smell of hydrogen sulfide (H_2S ; “rotten egg smell”). We suggest that the gypsum precipitation in the veins of the Rusayl Formation is due to the interaction of percolating calcium-bearing fluids. The H_2S of the Rusayl shales formed gypsum ($CaSO_4 \cdot 2H_2O$) under oxidizing conditions. The shale bed in Unit 1 does not smell like H_2S . The gypsum veins likely formed by precipitation from ascending fluids of corresponding mineralization from the Rusayl Formation. In years of continuous field work in the Oman Mountains, we have observed that gypsum veins are always associated with the Rusayl Formation and with the underlying Jafnayn and Al-Khod formations but also with the lower part of the Seeb Formation. Gypsum veins are also associated with fault mineralizations that occur in proximity to these formations (e.g., Figure 8 of [67]).

The thick brownish/purplish shale bed of sections 2 and 4 is mineralogically indistinguishable from the shale in the upper part of the Rusayl Formation (Table 1A–C). Therefore, we suggest, along with Beavington-Penney et al. [7], that the shale in Unit 1 is a recurrence

of the same facies as in the subjacent Rusayl Formation. We found no specific indication in support of a terra rossa interpretation. We are doubting this interpretation based on the absence of hematite and goethite in the XRD samples and on the critical comments provided by Dill et al. [17] (see text Section 4.3).

Mobile shale migration requires a high amount of water/fluid content (e.g., [68,69]). This seems more plausible for marine shales than for terra rossa paleosols. The lack of marine and terrestrial biota in the shale is inconclusive as to its depositional environment (marine? terra rossa?).

The onset of the deposition of the Seeb Formation (Unit 1) represents a marked change from fine-grained siliciclastic materials of the Rusayl Formation to limestones and is associated with a local concentration of gutter casts, followed by slumps and debrites. If the onset of deposition of Unit 1 occurred at 47.8 Ma or sometime later during the “basal Lutetian” (Section 1), it must have coincided with the relatively slow and steady cooling of the Saih Hatat Dome [37] and likely also the northern part of the Jabal Nakhl Subdome. At that time, the Jabal Akhdar area was heating up until 44 Ma [37]. Rapid uplift of the Jabal Akhdar Dome started at ~40 Ma [37], before 43 Ma [36] or at 43 Ma [38] and lasted until ~30 Ma [37]. We suggest that the slope gradient had initially changed at the onset of deposition of Unit 1 due to uplift of the Saih Hatat Dome and the northern part of the Jabal Nakhl Subdome. Later, doming of the Jabal Akhdar area became important.

While uplift occurred, the long-term eustatic sea-level curve indicates a steady rise of the sea level from 55 to 39 Ma [19], ensuring that marine limestone deposition could continue. An implication of this uplift and the eustatic sea-level history is that the shale in the upper Rusayl Formation, which accumulated before uplift, is likely a marine sediment. The thickness increase of Unit 1 to the SE (Table 2, Figures 18 and 19) is attributed to less overall uplift in SE direction (slow and steady cooling of the Saih Hatat Dome) than towards the West (Jabal Akhdar Dome). This could explain the availability of more accommodation space towards the SE, and thus, greater thickness and the greater influx of terrigenous quartz detritus in the NW than in the SE.

The migrating shale conforms to the definition of “mobile shale” *sensu* Morley and Guerin (1996) and Soto et al. (2021a). The presence of fluid for migration of mobile shale is a significant factor [68–73]. We saw no indication that shear played a role in mobilizing the shale of Unit 1. Instead, a high water/fluid content of the shale of Unit 1 is considered, taking into account the limited overburden of the Seeb Formation (Figure 1) and the related low loss of pore and interlayer water due to the shallow burial (water loss diagram for muddy sediments with increasing depth (Figure 3.8 of [58])). We are also encouraged to suggest a high water/fluid content as previous research showed that shales in the upper part of the Al-Khod Formation of Oman had a post-migration water/fluid loss of ~35 to 45% [69].

The high-water content had two effects. It caused a low shear strength of the shale and, thus, furthering its visco-plastic mobility. It also increased the density inversion between the shale bed and the overlying limestone beds. Density inversion may be considered, taking into account that the mobile shale moved upward in the stem of the shale tongue and that the shale tongue bulged the overlying limestone beds upwards (Figure 16A,B).

Section 4 with the shale tongue is associated with extensional faults. In fact, shale movement may have been triggered by fault activities, as reported similarly for the deformation of the Tertiary Ridge [55] and the formation of shale dike in the Al-Khod Formation [69]. This deformation interval seems to be the most important regional tectonic episode after deposition of the Seeb Formation. We suggest that the shale migration was triggered by corresponding post-“mid”-Eocene E-W convergence between Arabia and India [14,54] and related seismic tremors and faulting. Less likely, it was related to more local effects of the second faulting interval of the Frontal Range Fault [12,38].

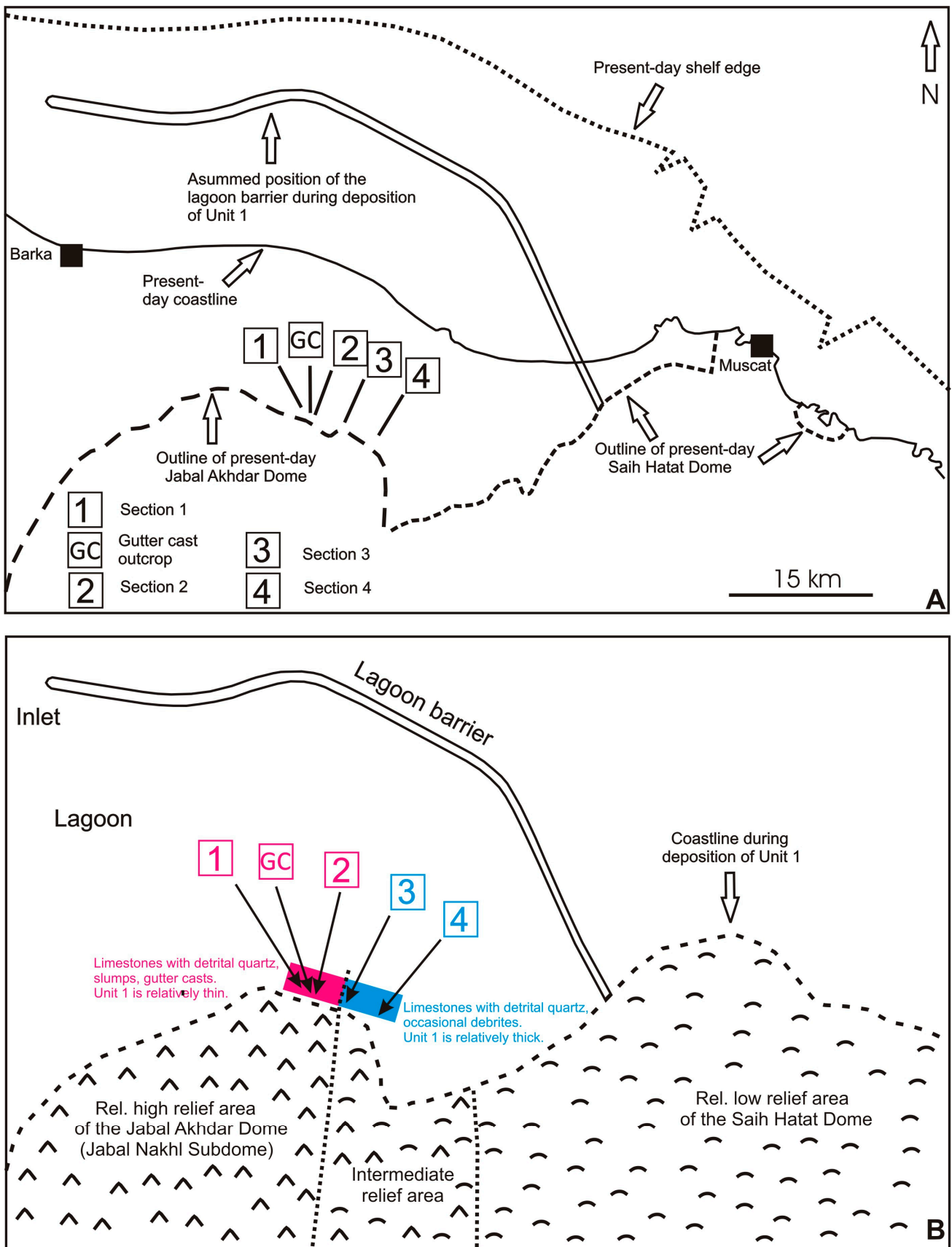


Figure 19. Paleogeographic model for the deposition of Unit 1, inspired by Nolan et al. [1] and Mattern et al. [45]. (A) Map sketch of the modern shelf edge, coastline and outline of the northernmost

Jabal Akhdar (Jabal Nakhil Subdome) and Saih Hatat domes. The position of the Early Eocene lagoon barrier is parallel to shelf edge and coastline. Within the barrier, a few present-day small islands with Miocene limestones/reef limestones occur [6], possibly indicating the presence of an elongated “high” (barrier?) in the geologic history. (B) Map sketch of the paleogeography during deposition of Unit 1. The western Jabal Nakhil area was uplifted more than the eastern Saih Hatat region. This may explain thickness differences within Unit 1 (more accommodation space in the eastern sections 3 and 4 compared to that of the western sections).

6. Conclusions

According to SMF evidence, Unit 1, at the base of the Seeb Formation, accumulated in a restricted, lagoonal setting, exhibiting a thickness increase towards the ESE. Differential uplift on the main land controlled this thickness trend due to differential accommodation space. The uplift also caused the influx of terrigenous quartz material. Shale from a shale bed in the upper part of Unit 1 shows evidence of post-depositional ductile migration.

The limestone microfacies are quite uniformly developed in Unit 1, with some textural differences (grainstones versus packstones) and compositional differences (benthic foraminifera versus peloids). Beavington and Penney et al. [7] suggested a low intertidal to shallow subtidal environment, whereas we found two dominant SMF types with fauna and flora typical for restricted, lagoonal conditions with water depths ranging from below one meter to a few meters or tens of meters with common terrigenous influx (FZ8; [18]). At a local scale, a beach-to-intertidal setting *sensu* Hersi and Al-Harthy [8] could well be possible.

The limestones reflect a uniform, lagoon-like depositional water depth rather than a noticeable and systematic increase in bathymetry in one direction as one would expect on a carbonate ramp. The commonly occurring SMF 16 has no direct equivalent on carbonate ramp microfacies (RMF; [18]), also suggesting that Unit 1 was deposited in a lagoon on a rimmed shelf rather than on a carbonate ramp as initially suggested by Racey [3]. At the same time, our data neither support the idea of an open, carbonate shelf *sensu* Nolan et al. [1] nor the interpretation of occasional supratidal environments *sensu* Dill et al. [17]. The scarcity of corals suggests that only small coral colonies existed in the lagoon without reaching the dimensions of patch reefs as defined by Mattern et al. [74].

The concluded lagoonal environment raises the question as to what the barrier of the lagoon was composed of. A coral barrier reef appears to be an unlikely option taking into account the scarcity of coral remains (seen in only three thin sections). Quartz sand and gravel also seem to be an unrealistic alternative for a shoal barrier due to their limited volume. Ooids can also be ruled out as potential material for a shoal barrier as they are absent in the samples. The abundance of benthic foraminifera, however, suggests that they were the main contributor to the formation of a lagoonal barrier as barrier islands and shoals. In particular, nummulite accumulations, together with echinoid fragments, benthic foraminifera such as *Discocyclina* and *Assilina*, smaller benthic foraminifera, calcareous red algae and molluscan debris that generally form banks or shoals in the Seeb Formation ([16]; see also [1,7]) are prime candidates that could have protected the lagoon in the form of shoal bodies. As the only SMF evidence for open marine conditions was found at the top of Section 1, which is the northwesternmost section, we conclude that the lagoon there was connected to the open sea (Figure 19B).

Gutter casts, slumps and debrites indicate the presence of a slope and slope instability, respectively. Initial slope formation is related to uplift of the Saih Hatat Dome and the northern area of the Jabal Nakhil Subdome [36,37]. While uplift occurred, the long-term eustatic sea-level curve rose. Towards the SE, the thickness increases (Table 2, Figures 18 and 19) due to overall lesser uplift of the Saih Hatat Dome [37] compared to that of the Jabal Akhdar Dome, which resulted in more accommodation space in the SE in the long run.

Author Contributions: Conceptualization: F.M.; formal analysis: F.M., A.S., A.R.A.-S., N.A.-W., L.G., G.F. and M.A.-S.; methodology: F.M., A.R.A.-S., N.A.-W., L.G., G.F. and M.A.-S.; formal analysis: F.M., A.S., A.R.A.-S., N.A.-W., L.G., G.F. and M.A.-S.; investigation: F.M., A.S., A.R.A.-S., N.A.-W., L.G., G.F. and M.A.-S.; writing—original draft preparation: F.M.; writing, review and editing: F.M., A.S., L.G. and G.F.; visualization: F.M. and A.S.; supervision: F.M. All authors have read and agreed to the published version of the manuscript.

Funding: This research received no external funding.

Acknowledgments: Nada Al-Wahaibi investigated Unit 1 in the Al-Khod area as part of her Final Year Research Project as a student at Sultan Qaboos University. We thank five anonymous reviewers and Editor Olivier Lacombe for their constructive reviews of the manuscript, and we thankfully acknowledge the preparation of thin-sections and XRD samples by Hamdan Al-Zidi (SQU). We are grateful to Sarah Mattern for improving the English text. The XRD samples were analyzed by the Central Analytical and Applied Research Unit (CAARU) at SQU.

Conflicts of Interest: The authors declare no conflict of interest.

Appendix A

Table A1. Condensed microscopic sample information of Section 1 for quick reference from base (Sample E) to top (Sample RAS). The relative frequency of bioclasts and other allochems is indicated. Limestones with 10–50% quartz sand are considered “quartz arenitic limestones” (no true limestones), and their SMF/FZ information is written in parentheses.

Sample	Rock Classification	Contents of Bioclasts, Other Allochems, Detrital Quartz	SMF/FZ
RAS (Top)	Red algae boundstone	Encrusting red algae, few branching red algae > bivalves > benthic foraminifera Some peloids and cortoids 1% of angular very fine to fine quartz sand	SMF 7 FZ 7
H	Foraminiferal pack- to grainstone, if detrital quartz content of >10% is not considered; quartz arenitic limestone (no true limestone)	Benthic foraminifera, including > echinoids, including corona plates and spines > branching red algae and <i>Distychoplax biserialis</i> > dasycladaceans Common peloids, few relatively large cortoids 15% of angular to subrounded fine to medium quartz sand	(SMF 18-FOR FZ 8)
G	Foraminiferal pack- to grainstone	Benthic foraminifera > encrusting and branching red algae > bivalves = echinoids, including spines = dasycladaceans Few peloids 5% angular very fine to fine quartz sand	SMF 18-FOR FZ 8
F	Fine-grained peloidal grainstone	Benthic foraminifera > bivalves > branching red algae > echinoid spines Abundant peloids, few relatively large cortoids 3% angular well-sorted very fine quartz sand	SMF 16-NON-LAMINATED FZ 8
I	Fine-grained peloidal grainstone	Benthic foraminifera > branching red algae > echinoids, including spines > bivalves > ostracods Abundant peloids, few cortoids 1% of angular to subrounded very fine to fine quartz sand	SMF 16-NON-LAMINATED FZ 8
K	Fine-grained foraminiferal grainstone	Benthic foraminifera > branching red algae > echinoids, including spines > gastropods = ostracods Some peloids, rare cortoids 7% of subrounded to angular fine to medium quartz sand	SMF 18-FOR FZ 8

Table A1. Cont.

Sample	Rock Classification	Contents of Bioclasts, Other Allochems, Detrital Quartz	SMF/FZ
D	Foraminiferal grainstone	Benthic foraminifera > echnoids, including spines > branching red algae > bivalves > dasycladaceans Some peloids, rare cortoids 5% of angular to subrounded fine to medium quartz sand	SMF 18-FOR FZ 8
A	Foraminiferal grainstone	Benthic foraminifera > echinoids, including spines > dasycladaceans > branching red algae > bivalves > gastropods Some peloids, rare cortoids <0.5% of angular medium quartz sand	SMF 18-FOR FZ 8
B	Fine-grained peloidal grainstone	Benthic foraminifera > echinoids > bivalves > ostracods > dasycladaceans Abundant peloids, few cortoids 2% angular to subrounded fine to coarse angular (1.3 mm max.) quartz sand; one quartzite clast of 1.1 mm	SMF 16-NON-LAMINATED FZ 8
C	Foraminiferal grainstone	Benthic foraminifera > echnoids, including spines > ostracods > dasycladaceans > Some peloids, few cortoids 2% of subrounded to angular (1 mm max.) fine to coarse quartz sand	SMF 18-FOR FZ 8
L	Fine-grained foraminiferal grainstone	Benthic foraminifera > bivalves > ostracods > echinoids, including spines > dasycladaceans Some peloids, few cortoids 2% of angular very fine to fine quartz sand	SMF 18-FOR FZ 8
J	Foraminiferal grainstone	Benthic foraminifera > branching red algae > dasycladaceans > echinoids > bivalves Few peloids and cortoids 1% of subrounded to angular quartz fine to medium sand	SMF 18-FOR FZ 8
E (Base)	Fine-grained peloidal grainstone, if detrital quartz content of >10% is not considered; quartz arenitic limestone (no true limestone)	Benthic foraminifera > branching red algae > dasycladaceans > bivalves > echinoids, including spine > ostracods Abundant peloids and cortoids 12% subrounded to angular very fine to medium quartz sand	(SMF 16-NON-LAMINATED FZ 8)

Appendix B

Table A2. Condensed microscopic sample information of Section 2 for quick reference from base (Sample 2) to top (Sample 9). The relative frequency of bioclasts and other allochems is indicated. Limestones with 10–50% quartz sand are considered “quartz arenitic limestones” (no true limestones), and their SMF/FZ information is written in parentheses.

Sample	Rock Classification	Contents of Bioclasts, Other Allochems, Detrital Quartz	SMF/FZ
9 (Top)	Laminated foraminiferal grain- to packstone (alternating laminae)	Benthic foraminifera > echinoderms > dasycladaceans > bivalves > ostracods > branching red algae > gastropods Some peloids, few cortoids 1% of angular to subrounded very fine to medium quartz sand	SMF 18-FOR FZ 8

Table A2. Cont.

Sample	Rock Classification	Contents of Bioclasts, Other Allochems, Detrital Quartz	SMF/FZ
8	Peloidal grainstone	Benthic foraminifera > echinoderms > dasycladaceans > red algae = bivalves Abundant peloids, some cortoids 1% of angular to subrounded very fine to medium quartz sand	SMF 16-NON-LAMINATED FZ 8
1	Fine-grained peloidal grainstone	Benthic foraminifera > echinoids > ostracods > branching red algae > dasycladaceans > bivalves Abundant peloids, some cortoids 1% angular, very well-sorted very fine quartz sand	SMF 16-NON-LAMINATED FZ 8
5	Laminated fine-grained, quartz-bearing peloidal packstone	Echinoids > benthic foraminifera > red algae Abundant peloids, some cortoids 15% angular silt to fine quartz sand	SMF 16-LAMINATED FZ 8
6	Foraminiferal grainstone, if detrital quartz content is not considered; quartz arenitic limestone (no true limestone)	Benthic foraminifera > dasycladaceans and other green algae > echinoids > bivalves > gastropods = ostracods Some peloids, cortoids and intraclasts 1% angular well-sorted fine quartz sand	(SMF 18-FOR FZ 8)
3	Foraminiferal grainstone	Benthic foraminifera > echinoids > red alga <i>Distychoplax biserialis</i> > dasycladaceans = bivalves Some peloids, few cortoids 3% angular fine to medium quartz sand, one 2.2 mm long quartzite granule	SMF 18-FOR FZ 8
10	Laminated peloidal packstone to grainstone, if detrital quartz content of >10% is not considered; quartz (no true limestone) arenitic limestone (no true limestone)	Echinoids > benthic foraminifera > dasycladaceans > branching red algae > ostracods Abundant peloids, some cortoids Angular very fine to medium quartz sand up to 20% in certain laminae (overall 15%)	(SMF 16-LAMINATED FZ 8)
4	Foraminiferal grainstone	Benthic foraminifera > branching red algae > echinoids > bivalves > dasycladaceans > ostracods Some peloids and cortoids 1% of angular very fine to medium quartz sand	SMF 18-FOR FZ 8
2 (Base)	Laminated foraminiferal grain-to packstone (alternating laminae)	Benthic foraminifera > echinoids > branching red algae and <i>Distychoplax biserialis</i> > dasycladaceans > ostracods Some peloids and cortoids 5% very well-sorted very fine angular quartz sand	SMF 18-FOR FZ 8

Appendix C

Table A3. Condensed microscopic sample information of Section 3 for quick reference from base (Sample S1) to top (Sample S11). The relative frequency of bioclasts and other allochems is indicated. Limestones with 10–50% quartz sand are considered “quartz arenitic limestones” (no true limestones), and their SMF/FZ information is written in parentheses.

Sample	Rock Classification	Contents of Bioclasts, Other Allochems, Detrital Quartz	SMF/FZ
S11 (Top)	Peloidal grainstone	Benthic foraminifera in relatively coarse-grained laminae > echinoid fragments, including spines > dasycladaceans > encrusting and branching red algae > ostracods Abundant peloids, few cortoids 1% of angular to subrounded fine to medium quartz sand	SMF 16-LAMINATED FZ 8

Table A3. Cont.

Sample	Rock Classification	Contents of Bioclasts, Other Allochems, Detrital Quartz	SMF/FZ
S12	Peloidal grainstone	Benthic foraminifera > echinoid fragments, including spines > bivalves > dasycladaceans > branching red algae and <i>Distychoplax biserialis</i> > ostracods Common peloids, some cortoids 1% of angular to subrounded fine to medium quartz sand	SMF 16-LAMINATED FZ 8
S8	Peloidal grainstone	Benthic foraminifera > echinoid fragments > dasycladaceans > bivalves > branching red algae Abundant peloids, some cortoids 5% angular to subrounded fine to medium quartz sand	SMF 16-NON-LAMINATED FZ 8
S10	Foraminiferal grainstone	Benthic foraminifera > echinoid fragments, including spines > dasycladaceans > ostracods Some peloids, few cortoids; one lamina of peloidal grainstone <1% of angular, well-sorted fine quartz sand	SMF 18-FOR FZ 8
S9	Foraminiferal grainstone	Benthic foraminifera > echinoid fragments, including corona plates and spines > dasycladaceans > ostracods > gastropods > branching red algae Common peloids, few cortoids 1% of angular to subrounded fine quartz sand	SMF 18-FOR FZ 8
S6	Partly dolomitized peloidal grainstone	Only few bioclasts; benthic foraminifera > echinoderm fragments > bivalves Abundant peloids, few rare large cortoids 2% of angular to subrounded fine to medium quartz sand	SMF 16-NON-LAMINATED FZ 8
S7	Mostly dolosparite	Relicts of bioclasts are echinoid fragments, rare micritic-walled red algae and what appear to be micritic-walled foraminifera 5% of angular to subrounded fine to medium quartz sand	No SMF/FZ assigned
S17	Peloidal grainstone	Benthic foraminifera > echinoid fragments, including corona plates and spines > poritid corals > gastropods > dasycladaceans Common peloids, few cortoids 5% angular to subrounded medium to coarse quartz and quartzite sand	SMF 16-NON-LAMINATED FZ 8
S16	Quartz-foraminiferal rudstone, if detrital quartz content of >10% is not considered (no true limestone)	Benthic foraminifera > echinoid fragments, including corona plates > gastropods > bivalves > dasycladaceans Some large cortoids, few peloids 18% angular to subrounded fine to coarse quartz sand and a few quartzite clasts with lengths <2.5 mm	-
S5	Foraminiferal grainstone (to rudstone)	Benthic foraminifera > echinoid fragments > dasycladaceans > ostracods = poritid corals = branching red algae and <i>Distychoplax biserialis</i> Rare large cortoids 1% angular to subrounded very coarse quartz sand (up to 2 mm), including quartzite fragments with 1.7 mm diameter	SMF 18-FOR FZ 8
S4	Foraminiferal grainstone	Benthic foraminifera > echinoderm fragments, including corona plates > dasycladaceans > branching red algae Some peloids, few cortoids 3% of angular to subangular medium quartz sand	SMF 18-FOR FZ 8
S3	Peloidal grainstone	Benthic foraminifera > echinoid fragments, including corona plates and spines > gastropods > bivalves > branching red algae Abundant peloids 5% of angular to subrounded fine to medium quartz sand	SMF 16-LAMINATED FZ 8

Table A3. Cont.

Sample	Rock Classification	Contents of Bioclasts, Other Allochems, Detrital Quartz	SMF/FZ
S2	Foraminiferal grainstone (to rudstone)	Benthic foraminifera > echinoid fragments, including corona plates and spines > dasycladaceans > branching red algae Few peloids 2% angular to subrounded quartz fine to medium sand	SMF 18-FOR FZ 8
S13	Foraminiferal grainstone	Benthic foraminifera > echinoid fragments, including corona plates and spines > gastropods > dasycladaceans > branching red algae > ostracods Some peloids, few cortoids 2% subrounded to angular fine to coarse quartz sand	SMF 18-FOR FZ 8
S1 (Base)	Laminated foraminiferal grainstone	Benthic foraminifera > echinoids, including corona plate fragments and spines > ostracods > bryozoans = bivalves > red algae, including <i>Distychoplax biserialis</i> Some peloids 3% angular to subrounded fine to coarse quartz sand	SMF 18-FOR FZ 8

Appendix D

Table A4. Condensed microscopic sample information of Section 4 from base (Sample AF1) to top (Sample AF22). The relative frequency of bioclasts and other allochems is indicated. Limestones with 10–50% quartz sand are considered “quartz arenitic limestones” (no true limestones), and their SMF/FZ information is written in parentheses.

Sample	Rock Classification	Contents of Bioclasts, Other Allochems, Detrital Quartz	SMF/FZ
AF22 (Top)	Partly dolomitized foraminiferal grainstone	Benthic micritic foraminifera and ghosts of foraminifera > corals > echinoids, including spines > branching red algae > ostracods Common peloids, few cortoids, two mainly calciclastic lithoclasts with angular medium quartz sand 4% angular to subangular fine to medium quartz sand	SMF 18-FOR FZ 8
AF21	Peloidal grainstone	Benthic foraminifera > echinoids, including spines Common peloids 7% subangular to subrounded very fine to medium quartz sand	SMF 16-NON-LAMINATED FZ 8
AF20	Peloidal grainstone	Benthic foraminifera > echinoids, including spines > bivalves > <i>Distychoplax biserialis</i> Common peloids 7% subangular to subrounded very fine to coarse quartz sand	SMF 16-NON-LAMINATED FZ 8
AF18	Foraminiferal grainstone; parallel orientation of bladed and elongate grains	Benthic foraminifera > echinoids, including spines > dasycladaceans Common peloids, some cortoids 2% subangular to subrounded very fine to very coarse quartz sand	SMF 18-FOR FZ 8
AF17	Peloidal grainstone	Benthic foraminifera > echinoids, including spines > encrusting and branching red algae > ostracods Abundant peloids, few large cortoids 2% subangular to subrounded very fine to medium quartz sand	SMF 16-LAMINATED FZ 8

Table A4. Cont.

Sample	Rock Classification	Contents of Bioclasts, Other Allochems, Detrital Quartz	SMF/FZ
AF16	Peloidal grainstone	Benthic foraminifera > echinoids, including spines > ostracods Abundant peloids, common cortoids (some large)	SMF 16-NON-LAMINATED FZ 8
AF15	Calcitic dolosparite with small dolomite crystals; developed from foraminifer grainstone	Benthic foraminifera (mainly with micritic tests) > echinoids > red algae Few large cortoids	SMF 18-FOR FZ 8
AF14	Peloidal grainstone	Rare echinoids Abundant peloids, some cortoids 1–2% angular to subrounded very fine to fine quartz sand	SMF 16-NON-LAMINATED FZ 8
AF13	Foraminiferal grainstone	Benthic foraminifera > echinoids, including spines > dasycladaceans > encrusting red algae Common peloids, some cortoids, rare intraclasts 5% subangular to subrounded medium to very coarse quartz/quartzite sand	SMF 18-FOR FZ 8
AF12	Porous, poorly cemented quartz-rich litharenite; cement is opaque material	90% very fine to very coarse quartz sand; lithics: quartzite, muscovite-quartz aggregates, chert	-
AF11	Peloidal grainstone; elongate grains are parallel, forming preferred orientation	Benthic foraminifera > echinoids, including spines > dasycladaceans > gastropods > ostracods Abundant peloids 5% angular to subrounded fine sand to granule-sized quartz grains which may be polycrystalline	SMF 16-NON-LAMINATED FZ 8
AF10	Peloidal grainstone	Benthic foraminifera > echinoids, including spines Abundant peloids, rare large cortoids 2% of very fine to medium angular to subangular quartz sand	SMF 16-NON-LAMINATED FZ 8
AF9	Peloidal grainstone	Echinoids, including spines > benthic foraminifera > dasycladaceans > ostracods Common peloids (including pellets?) 1–2% of angular very fine to fine angular to subangular quartz sand	SMF 16-NON-LAMINATED FZ 8
AF8	Locally dolomitized, foraminiferal biosparite; only few grain contacts	Benthic foraminifera = echinoids, including corona plates > branching red algae > dasycladaceans Few peloids, rare large cortoids 3–4% angular to subrounded very fine to medium quartz sand	-
AF7	Foraminiferal grainstone	Benthic foraminifera > echinoids, including corona plates > dasycladaceans > bivalves > gastropods > branching red algae > ostracods Few peloids	SMF 18-FOR FZ 8
AF6	Foraminiferal grainstone; in the field locally identified as rudstone	Benthic foraminifera, often flat, thin and disk-shaped > echinoids, including corona plates and test of sand dollar > dasycladaceans > branching red algae	SMF 18-FOR FZ 8
AF5	Foraminiferal grainstone from a debrite	Benthic foraminifera > echinoids, including corona plates > dasycladaceans > bivalves > gastropods Few peloids 2% angular to subrounded very fine to fine quartz sand	SMF 18-FOR FZ 8
AF4	Foraminiferal grainstone; parallel orientation of bladed and elongate grains	Benthic foraminifera > echinoids, including corona plates and spines > dasycladaceans > bivalves Few peloids, few large cortoids 3% angular to subrounded fine quartz sand	SMF 18-FOR FZ 8

Table A4. Cont.

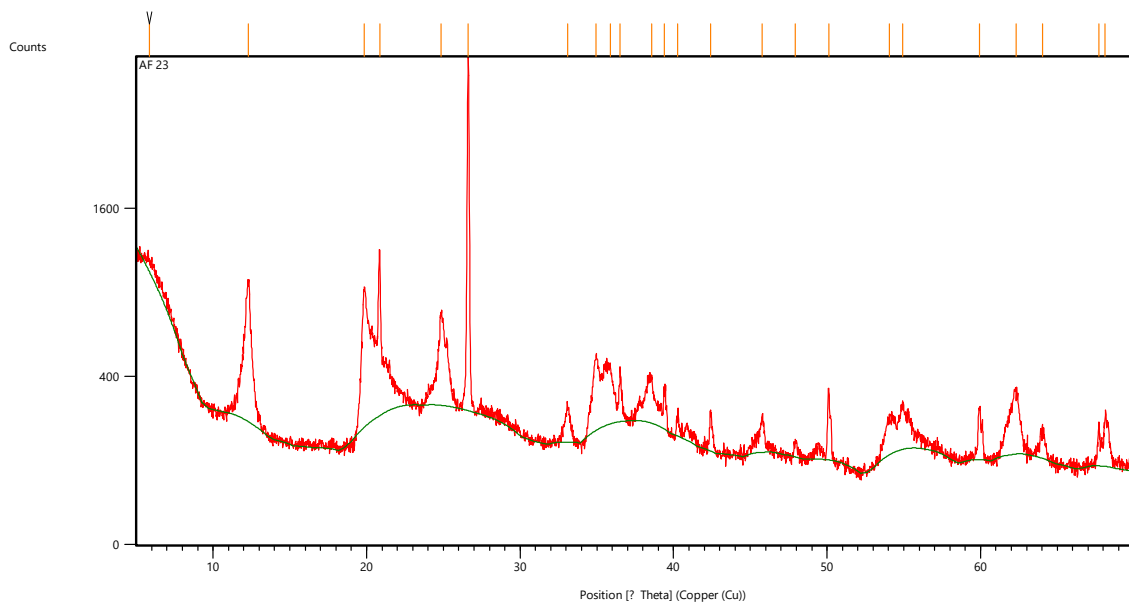
Sample	Rock Classification	Contents of Bioclasts, Other Allochems, Detrital Quartz	SMF/FZ
AF3	Matrix-supported biosparite; no grain contacts	Benthic foraminifera > echinoids, including test and spines > bivalves > dasycladaceans > branching red algae > gastropods > ostracods Few peloids, few large cortoids 3% angular to subangular very fine to fine quartz sand	-
AF2	Slightly dolomitized foraminiferal grainstone	Benthic foraminifera > branching red algae > echinoids, including corona plate > dasycladaceans = bivalves Some peloids, few large cortoids 1–2% of angular to subrounded very fine to fine quartz sand	SMF 18-FOR FZ 8
AF1 (Base)	Slightly dolomitized foraminiferal wackestone possibly slumped and/or bored	Benthic foraminifera > gastropods > bivalves > dasycladaceans > branching red algae Some peloids	-

Appendix E

XRD analysis of Sample AF23 (Section 2, Seeb Formation).

Ref. Code	Chemical Formula	Mineral Name	Wt%
98-015-6196	SiO ₂	Quartz	30
98-006-8698	Al ₂ Si ₂ O ₅ (OH) ₄	Kaolinite	70

Pos. [°2Th.]	Height [cts]	FWHM Left [°2Th.]	d-Spacing [Å]	Rel. Int. [%]
5.8591	104.88	0.6691	15.08452	3.42
12.3136	763.43	0.2342	7.18826	24.86
19.8315	722.97	0.2342	4.47698	23.55
20.8490	979.14	0.1004	4.26074	31.89
24.8411	476.85	0.2676	3.58433	15.53
26.6058	3070.43	0.1338	3.35046	100.00
33.1089	117.60	0.2676	2.70574	3.83
34.9313	304.11	0.2676	2.56864	9.90
35.8785	240.22	0.2676	2.50297	7.82
36.5170	206.43	0.1338	2.46066	6.72
38.5709	192.91	0.3011	2.33423	6.28
39.4121	149.18	0.1338	2.28633	4.86
40.2648	61.94	0.1673	2.23985	2.02
42.4104	135.54	0.1171	2.13137	4.41
45.7751	116.49	0.2007	1.98223	3.79
47.9358	41.44	0.2007	1.89781	1.35
50.0990	244.37	0.0836	1.82082	7.96
54.0590	102.43	0.5353	1.69642	3.34
54.9112	143.69	0.2007	1.67209	4.68
59.9179	160.77	0.1338	1.54379	5.24
62.2939	218.53	0.4015	1.49050	7.12
64.0282	68.57	0.3346	1.45425	2.23
67.6923	108.46	0.1004	1.38418	3.53
68.1186	144.58	0.1338	1.37655	4.71



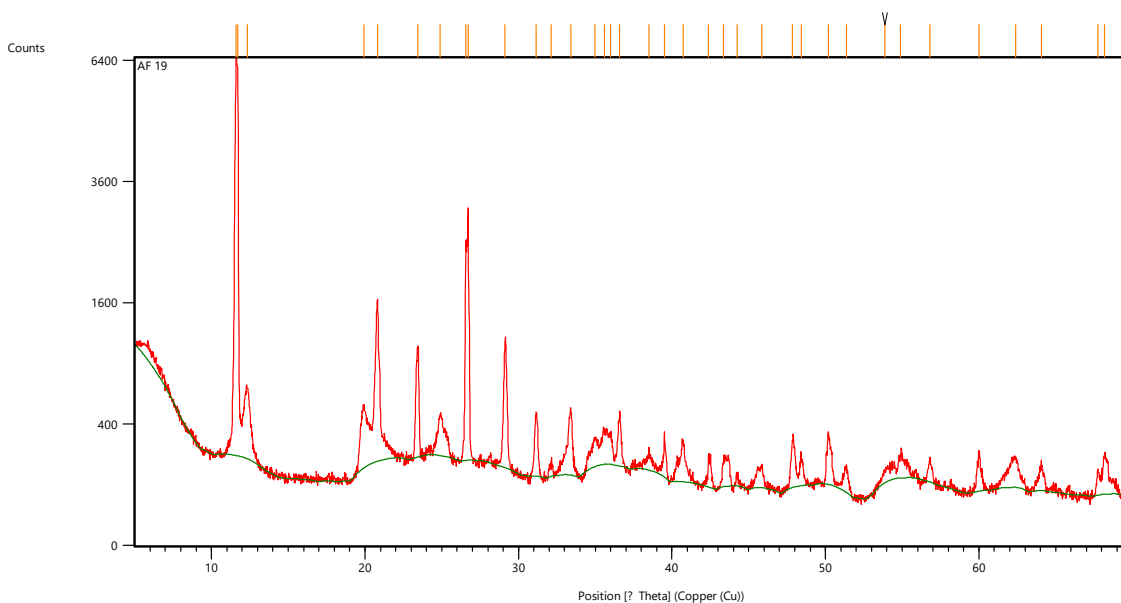
Appendix F

XRD analysis of Sample AF 19 (Section 4, Seeb Formation).

Ref. Code	Chemical Formula	Mineral Name	Wt%
98-008-3849	SiO ₂	Quartz	30
98-015-1692	CaSO ₄ ·2H ₂ O	Gypsum	45
98-006-8698	Al ₂ Si ₂ O ₅ (OH) ₄	Kaolinite	25

Pos. [°2Th.]	Height [cts]	FWHM Left [°2Th.]	d-Spacing [Å]	Rel. Int. [%]
11.5873	5848.54	0.1171	7.63710	100.00
11.7209	5188.75	0.0836	7.55034	88.72
12.3535	468.51	0.3011	7.16511	8.01
19.9105	359.62	0.3680	4.45940	6.15
20.8157	1429.30	0.1338	4.26748	24.44
23.4614	855.02	0.1171	3.79189	14.62
24.9063	250.29	0.2342	3.57509	4.28
26.5614	2236.08	0.0502	3.35595	38.23
26.7157	2895.81	0.0502	3.33692	49.51
29.1278	969.65	0.2175	3.06585	16.58
31.1332	344.10	0.1171	2.87279	5.88
32.1121	53.01	0.2007	2.78741	0.91
33.4179	366.67	0.2007	2.68143	6.27
34.9931	139.94	0.2676	2.56425	2.39
35.6026	173.75	0.3346	2.52173	2.97
36.0056	152.29	0.2007	2.49443	2.60
36.5950	300.24	0.2007	2.45560	5.13
38.4998	65.31	0.4015	2.33837	1.12
39.5183	221.50	0.0502	2.28043	3.79
40.7134	187.70	0.1338	2.21620	3.21
42.3806	113.60	0.2342	2.13280	1.94
43.3567	101.81	0.2007	2.08702	1.74
44.2390	33.89	0.2007	2.04743	0.58
45.8506	77.63	0.4684	1.97914	1.33

Pos. [°2Th.]	Height [cts]	FWHM Left [°2Th.]	d-Spacing [Å]	Rel. Int. [%]
47.8629	217.28	0.2342	1.90053	3.72
48.4222	116.39	0.2007	1.87988	1.99
50.1857	247.69	0.1004	1.81788	4.24
51.3475	91.70	0.2007	1.77944	1.57
53.8849	42.65	0.5353	1.70149	0.73
54.8889	101.91	0.2676	1.67272	1.74
56.8095	90.35	0.2676	1.62065	1.54
60.0097	152.36	0.2007	1.54165	2.61
62.3981	111.84	0.4684	1.48826	1.91
64.0828	93.21	0.2007	1.45314	1.59
67.7566	83.94	0.1338	1.38302	1.44
68.1690	148.15	0.1338	1.37565	2.53



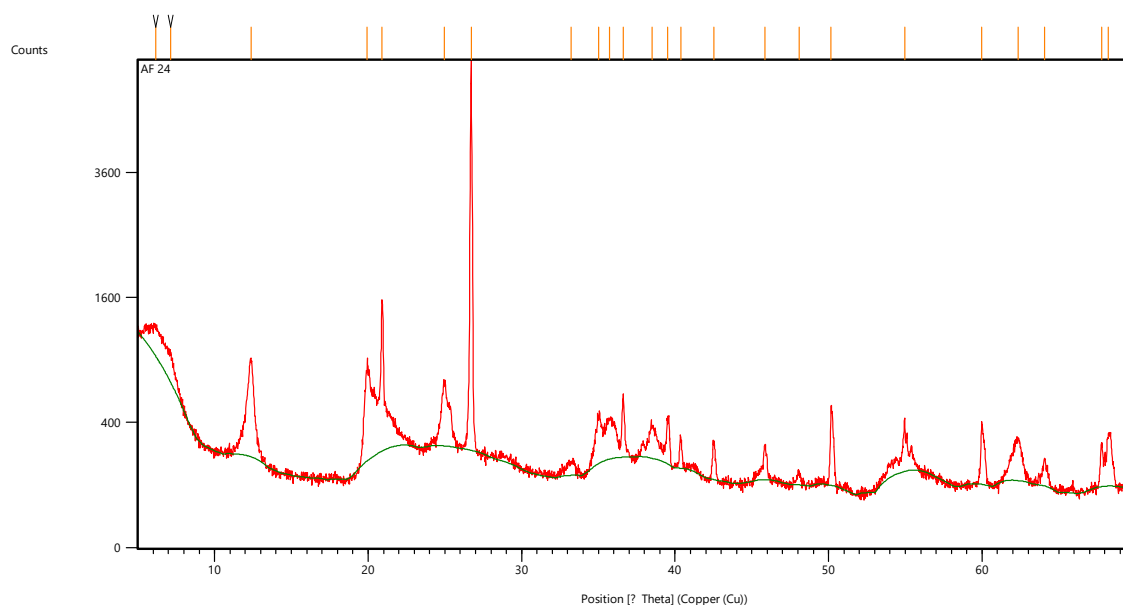
Appendix G

XRD analysis of Sample AF 24 (uppermost Rusayl Formation).

Ref. Code	Chemical Formula	Mineral Name	Wt%
98-002-7826	SiO ₂	Quartz	40
98-006-3316	Al ₂ Si ₂ O ₅ (OH) ₄	Kaolinite	60

Pos. [°2Th.]	Height [cts]	FWHM Left [°2Th.]	d-Spacing [Å]	Rel. Int. [%]
6.1646	313.51	0.5353	14.33751	5.34
7.1453	262.93	0.5353	12.37178	4.47
12.3956	684.43	0.2676	7.14086	11.65
19.9311	646.21	0.3346	4.45485	11.00
20.9094	1337.67	0.1338	4.24858	22.77
24.9880	438.33	0.2676	3.56359	7.46
26.7100	5875.77	0.1506	3.33762	100.00
33.2280	54.04	0.5353	2.69632	0.92
35.0156	248.20	0.2007	2.56265	4.22
35.7300	220.21	0.3346	2.51303	3.75

Pos. [°2Th.]	Height [cts]	FWHM Left [°2Th.]	d-Spacing [Å]	Rel. Int. [%]
36.6131	389.29	0.1004	2.45442	6.63
38.4790	170.79	0.2342	2.33959	2.91
39.5336	240.54	0.2007	2.27958	4.09
40.3574	154.89	0.1338	2.23493	2.64
42.5082	161.29	0.2007	2.12669	2.75
45.8392	157.18	0.1673	1.97961	2.68
48.0605	43.86	0.2007	1.89317	0.75
50.1578	415.08	0.1004	1.81882	7.06
54.9453	284.68	0.0612	1.66975	4.84
59.9850	299.44	0.1004	1.54222	5.10
62.3391	185.47	0.4015	1.48952	3.16
64.0834	103.17	0.3346	1.45313	1.76
67.7775	182.69	0.1338	1.38264	3.11
68.1994	215.99	0.1338	1.37512	3.68



References

- Nolan, S.C.; Skelton, P.W.; Clissold, B.P.; Smewing, J.D. Maastrichtian to Early Tertiary stratigraphy and paleogeography of the Central and Northern Oman Mountains. In *The Geology and Tectonics of the Oman Region*; Robertson, A.H.F., Ries, M.P., Ries, A.C., Eds.; Geological Society: London, UK, 1990; Volume 49, pp. 495–519.
- Jones, R.W.; Racey, A. Cenozoic stratigraphy of the Arabian Peninsula and Gulf. In *Micropaleontology and Hydrocarbon Exploration in the Middle East*; Simmons, M.D., Ed.; Chapman & Hall: London, UK, 1994; pp. 273–307.
- Racey, A. Lithostratigraphy and larger foraminiferal (nummulitid) biostratigraphy of the Tertiary of northern Oman. *Micropaleont.* **1995**, *41*, 1–123. [\[CrossRef\]](#)
- Schaub, H. Nummulites et Assilines de la Tethys paleogene, taxinomie, phylogenie et biostratigraphie avec deux volumes d'atlas. *Schweiz. Paläont. Abh.* **1981**, *104–106*, 236.
- Cohen, K.M.; Finney, S.; Gibbard, P.L. International Chronostratigraphic Chart (International Commission on Stratigraphy). *Episodes* **2013**, *36*, 199–204. [\[CrossRef\]](#) [\[PubMed\]](#)
- Béchenec, F.; Roger, J.; Le Métour, J.; Wyns, R. *Geological Map of Seeb, Sheet NF 40-03, 1:250,000 with Explanatory Notes*; Ministry of Petroleum and Minerals: Muscat, Oman, 1992.
- Beavington-Penney, S.J.; Wright, V.P.; Racey, A. The Middle Eocene Seeb Formation of Oman: An investigation of acyclicity, stratigraphic completeness, and accumulation rates in shallow marine carbonate settings. *J. Sediment. Res.* **2006**, *76*, 1137–1161. [\[CrossRef\]](#)
- Hersi, O.S.; Al-Harthy, A. Lithofacies attributes of a transgressive carbonate system: The middle Eocene Seeb formation, Al Khoudh area, Muscat, Oman. *SQU J. Sci.* **2010**, *15*, 41–54. [\[CrossRef\]](#)
- Pickford, M. Late Cretaceous Lanistes (Mollusca, Gastropoda) from Al-Khod, Oman. *Al-Hajar* **2017**, *23*, 15–29.

10. Mattern, F.; Al-Sayigh, A.R.; Farfour, M.; Scharf, A.; Al-Amri, S.; Al-Omairi, J. Microfacies, Biostratigraphy, Depositional Environment, Seismic Refraction and Correlation of Coralline Limestones of the Barzaman Formation (Oligocene-Pliocene? Al-Khod, Muscat Area, Oman). *SQU J. Sci.* **2020**, *25*, 85–99.
11. Callegari, I.; Scharf, A.; Mattern, F.; Scharf, K. Tectonic transition from thrusting to polyphase non-confining deformation within the Semail Ophiolite along the sinistral, transtensional Issmaïya Fault Zone (Sultanate of Oman). *J. Asian Earth Sci.* **2021**, *224*, 105007. [[CrossRef](#)]
12. Mattern, F.; Scharf, A. Postobductional extension along and within the Frontal Range of the Eastern Oman Mountains. *J. Asian Earth Sci.* **2018**, *154*, 369–385. [[CrossRef](#)]
13. Scharf, A.; Mattern, F.; Moraetis, D.; Callegari, I.; Weidle, C. Postobductional Kinematic Evolution and Geomorphology of a Major Regional Structure—The Semail Gap Fault Zone (Oman Mountains). *Tectonics* **2019**, *38*, 2756–2778. [[CrossRef](#)]
14. Scharf, A.; Mattern, F.; Bolhar, R.; Callegari, I.; Ring, U. Oligocene/early Miocene E/W-shortening in the Oman Mountains related to oblique Arabia-India convergence. *Tectonics* **2022**, *41*, e2022TC007271. [[CrossRef](#)]
15. Searle, M.P. Structural geometry, style and timing of deformation in the Hawasina window, Al Jabal al Akhdar and Saih Hatat culminations, Oman mountains. *GeoArabia* **2007**, *12*, 99–130. [[CrossRef](#)]
16. Racey, A. A review of Eocene nummulitide accumulations: Structure, formation and reservoir potential. *J. Petrol. Geol.* **2001**, *24*, 79–100. [[CrossRef](#)]
17. Dill, H.G.; Wehner, H.; Kus, J.; Botz, R.; Berner, Z.; Stüben, D.; Al-Sayigh, A. The Eocene Rusayl Formation, Oman, carbonaceous rocks in calcareous shelf sediments: Environment of deposition, alteration and hydrocarbon potential. *Int. J. Coal Geol.* **2007**, *72*, 89–123. [[CrossRef](#)]
18. Flügel, E. *Microfacies of Carbonate Rocks, Analysis, Interpretation and Application*, 2nd ed.; Springer: Berlin/Heidelberg, Germany, 2010; p. 984.
19. Haq, B.U.; Hardenbol, J.; Vail, P.R.; Wright, R.C.; Stover, L.E.; Baum, G.; Loutit, T.; Gombos, A.; Davies, T.; Pflum, C.; et al. Mesozoic-Cenozoic cycle chart. In *Sea-Level Changes: An Integrated Approach*; Wilgus, C.K., Hastings, B.S., Kendall, C.G.S., Posamentier, H.W., Ross, C.A., Van Wagoner, J.C., Eds.; SEPM: Tulsa, OK, USA, 1988.
20. Glennie, K.W.; Boeuf, M.G.A.; Hughes-Clarke, M.W.; Moody-Stuart, M.; Pilaar, W.F.H.; Reinhardt, B.M. Late Cretaceous nappes in Oman Mountains and their geological evolution. *Am. Assoc. Petrol. Geol. Bull.* **1973**, *57*, 5–27.
21. Glennie, K.W.; Boeuf, M.G.A.; Hughes-Clarke, M.W.; Moody-Stuart, M.; Pilaar, W.; Reinhardt, B.M. Geology of the Oman Mountains. *Verh. K. Ned. Geol. Mijnbouwkd. Genoot.* **1974**, *31*, 1–423. [[CrossRef](#)]
22. Searle, M.P.; Malpas, J. Structure and metamorphism of rocks beneath the Semail ophiolite of Oman and their significance in ophiolite obduction. *Trans. R. Soc. Edinb.* **1980**, *71*, 247–262. [[CrossRef](#)]
23. Lippard, S.J.; Shelton, A.W.; Gass, I.G. The ophiolite of northern Oman. *Geol. Soc. Mem.* **1986**, *11*, 1–178.
24. Goffé, B.; Michard, A.; Kienast, J.R.; LeMer, O. A case of obduction related high P, low T metamorphism in upper crustal nappes, Arabian continental margin, Oman: P-T paths and kinematic interpretation. *Tectonophysics* **1988**, *151*, 363–386. [[CrossRef](#)]
25. Rollinson, H.R.; Searle, M.P.; Abbasi, I.A.; Al-Lazki, A.I.; Al Kindi, M.H. (Eds.) Introduction. In *Tectonic Evolution of the Oman Mountains*; Geological Society: London UK, 2014; Volume 392, pp. 27–37.
26. Searle, M.; Cox, J. Tectonic setting, origin, and obduction of the Oman ophiolite. *Geol. Soc. Am. Bull.* **1991**, *111*, 104–122. [[CrossRef](#)]
27. Hacker, B.R.; Mosenfelder, J.L.; Gnos, E. Rapid emplacement of the Oman ophiolite: Thermal and geochronologic constraints. *Tectonics* **1996**, *15*, 1230–1247. [[CrossRef](#)]
28. Glennie, K.W. *The Geology of the Oman Mountains: An Outline of Their Origin*, 2nd ed.; Scientific Press: Beaconsfield, UK, 2005; p. 110.
29. Scharf, A.; Mattern, F.; Al-Wardi, M.; Frijia, G.; Moraetis, D.; Pracejus, B.; Bauer, W.; Callegari, I. *The Geology and Tectonics of the Jabal Akhdar and Saih Hatat Domes, Oman Mountains*; Geological Society: London, UK, 2021; Volume 54, p. 124.
30. Al-Wardi, M.; Butler, R.W.H. Constrictional extensional tectonics in the northern Oman mountains, its role in culmination development and the exhumation of the subducted Arabian continental margin. In *Deformation of the Continental Crust: The Legacy of Mike Coward*; Ries, A.C., Butler, R.W.H., Graham, R.H., Eds.; Geological Society: London, UK, 2007; Volume 272, pp. 187–202.
31. Scharf, A.; Bailey, C.M.; Bolhar, R.; Mattern, F.; Ring, U. Post-obduction listwaenite genesis in the Oman Mountains inferred from structural analysis and U-Pb carbonate dating. *Earth Planet. Sci. Lett.* **2022**, *595*, 117756. [[CrossRef](#)]
32. Coffield, D.Q. Structures associated with nappe emplacement and culmination collapse in the Central Oman Mountains. In *The Geology and Tectonics of the Oman Region*; Robertson, A.H.F., Ries, M.P., Ries, A.C., Eds.; Geological Society: London, UK, 1990; Volume 49, pp. 4547–4548.
33. Poupeau, G.; Saddiqi, O.; Goffé, A.M.B.; Oberhänsli, R. Late thermal evolution of the Oman Mountains subophiolitic windows: Apatite fission-track thermochronology. *Geology* **1998**, *26*, 1139–1142. [[CrossRef](#)]
34. Saddiqi, O.; Michard, A.; Goffé, B.; Poupeau, G.; Oberhänsli, R. Fission-track thermochronology of the Oman Mountains continental windows, and current problems of interpretation. *Bull. Soc. Géol. Fr.* **2006**, *177*, 127–134. [[CrossRef](#)]
35. Grobe, A.; Virgo, S.; von Hagke, C.; Urai, J.L.; Littke, R. Multiphase Structural Evolution of a Continental Margin during Obduction Orogeny: Insights from the Jebel Akhdar Dome, Oman Mountains. *Tectonics* **2018**, *37*, 888–913. [[CrossRef](#)]
36. Grobe, A.; van Hagke, C.; Littke, R.; Dunkl, I.; Wübbeler, F.; Muchez, P.; Urai, J.L. Tectono-thermal evolution of Oman's Mesozoic passive continental margin under the obducting Semail Ophiolite: A case study of Jebel Akhdar, Oman. *Solid Earth* **2019**, *10*, 149–175. [[CrossRef](#)]

37. Hansman, R.J.; Ring, U.; Thomson, S.N.; den Brock, B.; Stübner, K. Late Eocene uplift of the Al Hajar Mountains, Oman, supported by stratigraphic and low-temperature thermochronology. *Tectonics* **2017**, *36*, 3081–3109. [[CrossRef](#)]
38. Scharf, A.; Sudo, M.; Pracejus, B.; Mattern, F.; Callegari, I.; Bauer, W.; Scharf, K. Late Lutetian (Eocene) mafic intrusion into shallow marine platform deposits north of the Oman Mountains (Rusayl Embayment) and its tectonic significance. *J. Afr. Earth Sci.* **2020**, *170*, 103941. [[CrossRef](#)]
39. Abbasi, I.A.; Hersi, O.S.; Al-Harty, A. Late Cretaceous conglomerates of the Qahlah Formation, north Oman. In *Tectonic Evolution of the Oman Mountains*; Rollinson, H.R., Searle, M.P., Abbasi, I.A., Al-Lazki, A., Al-Kindi, M.H., Eds.; Geological Society: London, UK, 2014; Volume 392, pp. 325–341.
40. Keen, M.C.; Racey, A. Lower Eocene Ostracods from the Rusayl Shale Formation of Oman. *J. Micropal.* **1991**, *10*, 227–233. [[CrossRef](#)]
41. Özcan, E.; Abbasi, I.A.; Drobne, K.; Govindan, A.; Jovane, L.; Boukhalfa, K. Early Eocene orthophragminids and alveolinids from the Jafnayn Formation, N Oman: Significance of *Nemkovella stockari* Less & Özcan, 2007 in Tethys. *Geodin. Acta* **2016**, *28*, 160–184.
42. Serra-Kiel, J.; Vicedo, V.; Razin, P.; Grélaud, C. Selandian-Thanetian larger foraminifera from the lower Jafnayn formation in the Sayq area (eastern Oman Mountains). *Geol. Acta* **2016**, *14*, 315–333.
43. Tomás, S.; Frijia, G.; Bömelburg, E.; Zamagni, J.; Perin, C.; Mutti, M. Evidence for seagrass meadows and their response paleoenvironmental changes in the early Eocene (Jafnayn Formation, Wadi Bani Khalid, N Oman). *Sediment. Geol.* **2016**, *341*, 189–202. [[CrossRef](#)]
44. Mattern, F.; Bernecker, M. A shallow marine clinoform system in limestones (Paleocene/Eocene Jafnayn Formation, Oman): Geometry, microfacies, environment and processes. *Carbonates Evaporites* **2019**, *34*, 101–113. [[CrossRef](#)]
45. Mattern, F.; Scharf, A.; Al-Sarmi, M.; Al-Sayigh, A.R.; Al-Maktoumi, M.; Al-Omairi, N.; Al-Rawahi, T.; Al-Moqbali, M. Lithostratigraphy, microfacies and paleogeography of the shallow marine Middle Limestone Member of the Early Eocene Rusayl Formation, Oman: Relationship to the Early Eocene Climatic Optimum, sea-level changes and regional uplift. *J. Afr. Earth Sci.* **2021**, *184*, 104312. [[CrossRef](#)]
46. Mattern, F.; Al-Amri, S.; Scharf, A.; Al-Sayigh, A.R.; Farfour, M.; Pracejus, B.; Al-Omairi, J.; Callegari, I. Lithostratigraphy, facies, mineralogy and diagenesis of the syntectonic late Oligocene and Neogene Barzaman Formation (Al-Khod, Sultanate of Oman). *J. Afr. Earth Sci.* **2021**, *185*, 104416. [[CrossRef](#)]
47. Keating-Bitonti, C.R.; Ivany, L.C.; Affek, H.P.; Douglas, P.; Samson, S.D. Warm, not super-hot, temperatures in the early Eocene subtropics. *Geology* **2011**, *39*, 771–774. [[CrossRef](#)]
48. Kraus, M.J.; McInerney, F.A.; Wing, S.L.; Secord, R.; Baczynski, A.A.; Bloch, J.I. Paleohydrologic response to continental warming during the Paleocene–Eocene thermal maximum, bighorn basin, Wyoming. *Palaeogeogr. Palaeoclimatol. Palaeoecol.* **2013**, *370*, 196–208. [[CrossRef](#)]
49. Zachos, J.C.; Dickens, G.R.; Zeebe, R.E. An early Cenozoic perspective on greenhouse warming and carbon-cycle dynamics. *Nature* **2008**, *451*, 279–283. [[CrossRef](#)] [[PubMed](#)]
50. Speelman, E.N.; van Kempen, M.M.; Barke, J.; Brinkhuis, H.; Reichert, G.J.; Smolders, A.J.P.; Roelofs, J.G.M.; Sangiorgi, F.; de Leeuw, J.W.; Lotter, A.F.; et al. The Eocene Arctic *Azolla* bloom; environmental conditions, productivity and carbon drawdown. *Geobiology* **2009**, *7*, 155–170. [[CrossRef](#)]
51. Rego, E.S.; Jovane, L.; Hein, J.R.; Sant’Anna, L.G.; Giorgioni, M.; Rodelli, D.; Özcan, E. Mineralogical evidence for warm and dry climatic conditions in the Neo Tethys (eastern Turkey) during the middle Eocene. *Palaeogeogr. Palaeoclimatol. Palaeoecol.* **2018**, *501*, 45–57. [[CrossRef](#)]
52. Giorgioni, M.; Jovane, L.; Rego, E.S.; Rodelli, D.; Frontalini, F.; Catanzariti, R.; Özcan, E. Carbon cycle instability and orbital forcing during the Middle Eocene Climatic Optimum. *Sci. Rep.* **2019**, *9*, 9357. [[CrossRef](#)] [[PubMed](#)]
53. Van der Boon, A.; Kuiper, K.F.; van der Ploeg, R.; Cramwinckel, M.J.; Honarmand, M.; Sluijs, A.; Krijgsman, W. Exploring a link between the Middle Eocene Climatic Optimum and Neotethys continental arc flare-up. *Clim. Past* **2021**, *17*, 229–239. [[CrossRef](#)]
54. Mattern, F.; Bolhar, R.; Scharf, A.; Scharf, K.; Mattern, P.; Callegari, I. *Novelly Discovered Post-Mid-Eocene Sinistral Slip in the Eastern Oman Mountains: Widely Distributed Shear with Wrench-Fault Assemblage Related to Arabia-India Convergence*; EGU Abstract 2021 #8321; EGU (European Geosciences Union) General Assembly: Vienna, Austria, 2021.
55. Scharf, A.; Mattern, F.; Al Sadi, S. Kinematics of Post-obductional Deformation of the Tertiary Ridge at Al-Khod Village (Muscat Area, Oman). *SQU J. Sci.* **2016**, *21*, 26–40. [[CrossRef](#)]
56. Mattern, F. Compiled Synoptic Table of the Standard Microfacies and Facies Zone System of Flügel (2010): A Practical Tool. *SQU J. Sci.* **2022**, *27*, 74–76. [[CrossRef](#)]
57. Jackson, J.A. *Glossary of Geology*, 4th ed.; American Geological Institute: Alexandria, VA, USA, 1997; p. 769.
58. Jackson, M.P.A.; Talbot, C.J. Advances in Salt Tectonics. In *Continental Deformation*; Hancock, P.L., Ed.; Pergamon: Oxford, UK, 1994; pp. 159–179.
59. Tucker, M.E. *Sedimentary Petrology*, 3rd ed.; Blackwell: Oxford, UK, 2001; p. 262.
60. Serra-Kiel, J.; Gallardo-Garcia, A.; Razin, P.; Robinet, J.; Roger, J.; Grélaud, C.; Leroy, S.; Robin, C. Middle Eocene-Early Miocene larger foraminifera from Dhofar (Oman) and Socotra Island (Yemen). *Arab. J. Geosci.* **2016**, *9*, 344. [[CrossRef](#)]
61. Yaseen, A.; Munir, M.; Ur-Rehman, O.; Mirza, K. Microfacies analysis of the Middle Eocene Kohat Formation, Shekhan Nala, Kohat Basin, Pakistan. *Geol. Bull. Punjab Univ.* **2007**, *42*, 15–24.

62. Scholle, P.A.; Ulmer-Schuler, D.S. A Color Guide to the Petrography of Carbonate Rocks: Grains, Textures, Porosity, Diagenesis. *Am. Assoc. Pet. Geol. Mem.* **2003**, *77*, 459.
63. Adams, J.E.; Rhodes, M.L. Dolomitization by seepage reflux. *Am. Assoc. Petrol. Geol. Bull.* **1960**, *44*, 1912–1920.
64. Warren, J.K. Sulfate dominated sea-marginal and platform evaporative settings. In *Evaporites, Petroleum and Mineral Resources*; Melvin, J.L., Ed.; Dev. Sedimentol. 50; Elsevier: Amsterdam, The Netherlands, 1991; pp. 477–533.
65. Machel, H.G. Concepts and models of dolomitization: A critical reappraisal. In *The Geometry and Petrogenesis of Dolomite Hydrocarbon Reservoirs*; Braithwaite, C.J.R., Rizzi, G., Darke, G., Eds.; Geological Society: London, UK, 2004; Volume 235, pp. 7–63.
66. Pérez-López, A. Significance of pot and gutter casts in a Middle Triassic carbonate platform, Betic Cordillera, southern Spain. *Sedimentology* **2001**, *48*, 1371–1388. [[CrossRef](#)]
67. Mattern, F.; Scharf, A.; Pracejus, B.; Al Shibli, I.A.S.; Al Kabani, B.M.S.; Al Qasmi, W.Y.A.; Kiessling, W.; Callegari, I. Origin of the Cretaceous olistostromes in the Oman mountains (Sultanate of Oman): Evidence from clay minerals. *J. Afr. Earth Sci.* **2022**, *191*, 104547. [[CrossRef](#)]
68. Morley, C.K.; Guerin, G. Comparison of gravity-driven deformation styles and behavior associated with mobile shales and salt. *Tectonics* **1996**, *15*, 1154–1170. [[CrossRef](#)]
69. Mattern, F.; Scharf, A.; Al-Sarmi, M.; Pracejus, B.; Al-Hinaai, A.-S.; Al-Mamari, A. Compaction history of Upper Cretaceous shale and related tectonic framework, Arabian Plate, Eastern Oman Mountains. *Arab. J. Geosci.* **2018**, *11*, 444. [[CrossRef](#)]
70. Bruce, C.H. Pressured Shale and Related Sediment Deformation: Mechanism for the Development of Regional Contemporaneous Faults. *Amer. Assoc. Petrol. Geol. Bull.* **1973**, *57*, 878–886.
71. Soto, J.I.; Hudec, M.R.; Mondol, N.H.; Heidari, M. Shale transformations and physical properties—Implications for seismic expression of mobile shales. *Earth-Sci. Rev.* **2021**, *220*, 103746. [[CrossRef](#)]
72. Dinc, G.; Callot, J.-P.; Ringenbach, J.-C. Shale mobility: From salt-like shale flow to fluid mobilization in gravity-driven deformation, the late Albian–Turonian White Pointer Delta (Ceduna Subbasin, Great Bight, Australia). *Geology* **2023**, *51*, 174–178. [[CrossRef](#)]
73. Soto, J.I.; Heidari, M.; Hudec, M.R. Proposal for a mechanical model of mobile shales. *Sci. Rep.* **2021**, *11*, 23785. [[CrossRef](#)]
74. Mattern, F.; Moraetis, D.; Abbasi, I.; Al Shukaili, B.; Scharf, A.; Claereboudt, M.; Looker, E.; Al Haddabi, N.; Pracejus, B. Coastal dynamics of uplifted and emerged late Pleistocene near-shore coral patch reefs at fins (eastern coastal Oman, Gulf of Oman). *J. Afr. Earth Sci.* **2018**, *138*, 192–200. [[CrossRef](#)]

Disclaimer/Publisher’s Note: The statements, opinions and data contained in all publications are solely those of the individual author(s) and contributor(s) and not of MDPI and/or the editor(s). MDPI and/or the editor(s) disclaim responsibility for any injury to people or property resulting from any ideas, methods, instructions or products referred to in the content.